RI 9355

REPORT OF INVESTIGATIONS/1991

Elastic Wave Velocity and Attenuation as Used To Define Phases of Loading and Failure in Coal

By V. R. Shea-Albin, D. R. Hanson, and R. E. Gerlick

UNITED STATES DEPARTMENT OF THE INTERIOR

BUREAU OF MINES

Mission: As the Nation's principal conservation agency, the Department of the Interior has responsibility for most of our nationally-owned public lands and natural and cultural resources. This includes fostering wise use of our land and water resources, protecting our fish and wildlife, preserving the environmental and cultural values of our national parks and historical places, and providing for the enjoyment of life through outdoor recreation. The Department assesses our energy and mineral resources and works to assure that their development is in the best interests of all our people. The Department also promotes the goals of the Take Pride in America campaign by encouraging stewardship and citizen responsibility for the public lands and promoting citizen participation in their care. The Department also has a major responsibility for American Indian reservation communities and for people who live in Island Territories under U.S. Administration.

Report of Investigations 9355

Elastic Wave Velocity and Attenuation as Used To Define Phases of Loading and Failure in Coal

By V. R. Shea-Albin, D. R. Hanson, and R. E. Gerlick

UNITED STATES DEPARTMENT OF THE INTERIOR
Manuel Lujan, Jr., Secretary

BUREAU OF MINES
T S Ary, Director

Library of Congress Cataloging in Publication Data:

Shea-Albin, V. R.

Elastic wave velocity and attenuation as used to define phases of loading and failure in coal / by V.R. Shea-Albin, D.R. Hanson, R.E. Gerlick.

p. cm. — (Report of investigations; 9355)

Includes bibliographical references (p. 16).

Supt. of Docs. no.: I 28.23:9355.

1. Ground control (Mining) 2. Coal—Testing. 3. Fracture mechanics. I. Hanson, David R. II. Gerlick, R. E. III. Title. IV. Series: Report of investigations (United States. Bureau of Mines); 9355.

TN23.U43 [TN288] 622 s—dc20 [622'.334] 90-49808 CIP

CONTENTS

ILLUSTRATIONS

ILLUSTRATIONS—Continued

TABLE

UNIT OF MEASURE ABBREVIATIONS USED IN THIS REPORT

dB	decibel	MHz	megahertz
ft	foot	min	minute
ft/s	foot per second	mV	millevolt (volt × 10^{-3})
g/cm^3	gram per cubic centimeter	Ω	ohm
in	inch	psi	pound per square inch
in/s	inch per second	s	second
kHz	kilohertz	μs	microsecond (second × 10^{-6})
lb	pound	V	volt

ELASTIC WAVE VELOCITY AND ATTENUATION AS USED TO DEFINE PHASES OF LOADING AND FAILURE IN COAL

By V. R. Shea-Albin,[1] D. R. Hanson,[2] and R. E. Gerlick[3]

ABSTRACT

This U.S. Bureau of Mines report discusses elastic wave velocity and attenuation behavior as an indicator for changes in load and structural integrity of coal samples. Measuring changes in compressional (P)-wave and shear (S)-wave attenuation and velocity under uniaxial and triaxial compression tests revealed their effectiveness for distinguishing changes in applied load and structural failure of samples. The velocity and attenuation values were used in further calculations such as ratios of P-wave to S-wave values, dynamic elastic constants, normalized velocities, and attenuation coefficients to reveal trends for loading and failure.

The behavior of both P-wave and S-wave attenuation and velocity together define distinct and consistent phases of load change and failure for uniaxial and triaxial tests. The S-wave velocity and attenuation illustrate changing axial load and initial development of microfractures within the sample preceding structural failure more clearly than those of the P-wave. The attenuation and velocity ratios and dynamic elastic constants (except the bulk modulus) respond to closure of small preexisting fractures within the coal sample with initial loading to failure of coal samples. The attenuation coefficients and normalized velocities reveal trends similar to those shown by velocity and attenuation.

[1]Materials engineer.
[2]Geophysical engineer.
[3]Engineering technician.
Denver Research Center, U.S. Bureau of Mines, Denver, CO.

INTRODUCTION

This report describes the results of laboratory work performed as part of a U.S. Bureau of Mines research project, the purpose of which was to investigate nondestructive methods to locate and verify the extent of the yield zone and stress abutment peak in coal mine pillars. The yield zone refers to an outer envelope of failed coal defined by Wilson to be peripheral to an abutment zone of high stress within the pillar (*1-3*).[4] Measurement of the extent of this yield zone requires a method that is sensitive to both changes in stress and development of fractures within the coal.

The influence of fractures and change in stress upon attenuation and velocity of ultrasonic elastic waves travelling through a fractured and stressed medium is well documented (*4-13*), in particular, Su (*6*), Stacy (*10*), and Lockner (*11*). Thill (*12*), Molina (*13*), and Terry (*14*) obtained experimental results pertinent to the application of elastic wave attenuation and velocity used in this investigation. Stacy (*10*) determined that S-waves are more responsive than P-waves to irregularities such as fractures or voids within the rock. The properties he investigated include velocity, frequency, wavelength, and amplitude. Lockner (*11*) stated that ultrasonic wave attenuation is more sensitive than velocity to the formation of microfractures prior to failure in rock subjected to increasing levels of stress applied perpendicular to the direction of wave propagation. Molina (*13*) found that the closing of cracks by adding load to a core sample improved the coupling within the rock sample, increasing energy transmission through the sample as well as the velocity of the elastic waves. This trend continued with increasing load until applied stress began to cause the formation of new cracks within the sample, at which point energy transmission decreased. Terry (*14*) experimented with the effects of P-waves propagated through coal samples. Terry found that coal contained air-filled cracks, which he called "layer cavities," that are oriented parallel to bedding, and perpendicular to both the major and minor cleat. He found a greater increase of velocity upon initial loading in samples oriented perpendicular to bedding, indicating that the layer cavities had a more significant effect on velocity than either major or minor cleat.

Initial load applied parallel to wave propagation caused a nonlinear increase in velocity. Once the layer cavities were closed by load, the change of velocity was more linear with respect to increase in load. Su (*6*) investigated the effectiveness of P-wave velocities for measuring the magnitude and the direction of stresses surrounding boreholes drilled in sample blocks of rocks to which external stresses were applied. McKenzie (*8*) developed a cross borehole method of measuring P-wave velocity and attenuation to characterize the structural condition of rock in underground and surface mines. These collective results from the work of the two previous authors lead to the hypotheses for this investigation—that elastic wave velocity and attenuation would be effective for measurement of changes in stress and structural integrity with distance into a coal pillar accessed by a drill hole, and these laboratory results could be applied to field detection of the stress abutment peak and the yielded zone of a coal pillar.

The experiment was designed to build on the work previously described. Based on the work by Stacy (*10*), both S-waves and P-waves were propagated through coal samples. From the work by Lockner (*11*), the changes in both velocity and attenuation of the signals were measured. Similar to the procedure used by Molina (*13*), the experiment involved monitoring the change in the behavior of P-wave and S-wave velocity and attenuation in response to increase in load through sample failure. The testing conditions used in the laboratory experiment were chosen to simulate as closely as possible the conditions that would be found in a coal pillar. In a coal pillar, the principal stress is usually oriented perpendicular to bedding. The coal samples to be tested were, therefore, drilled perpendicular to bedding, and were loaded axially to simulate conditions within a coal pillar. The P-waves and S-waves were also propagated perpendicular to bedding and parallel to the direction of loading. This orientation of loading also provided the advantage that the presence of layer cavities parallel to the bedding in coal causes a greater change in velocity and attenuation of elastic waves upon initial loading, as Terry (*14*) found. Samples were tested at different confinement pressures to approximate confinement pressures within a coal pillar.

[4]Italic numbers in parentheses refer to items in the list of references preceding the appendix at the end of this report.

ACKNOWLEDGMENTS

The authors wish to express their gratitude to Bureau employees Robert Munson, geophysicist, for providing equipment for experimental setup and Thomas Rich, electronics technician, for design of electronic enhancements for the experimental setup.

TEST EQUIPMENT

As shown in figure 1, the experimental setup includes two 1-MHz Harisonic[5] P-wave and S-wave transducers. One transducer transmits the source signal through the coal sample, and the other receives the signal after it has travelled through the coal. A function generator supplies a 5-V square wave that triggers a Cober Electronics, Inc., Stamford, CT, high-powered function generator. This pulse drives the source transducer and provides a reference signal from which arrival times can be measured. Amplifiers and band pass filters amplify and filter the signal from the receiving transducer. The amplifier settings for both the P-wave and S-wave signal are 36 dB. The low-pass filter settings for both the P-wave and S-wave signal are 1,000 MHz. The high-pass filter for the P-wave signal is set at 10 kHz. The high-pass filter for the S-wave signal is set at 25 kHz. A four-channel digital storage oscilloscope displays the source signal on channel one, which serves as a reference, with the second and third channels displaying the received P-wave and S-wave signals, respectively, from the receiving transducer. The coal sample is held between steel platens in the load frame of a servocontrolled materials testing system (MTS), which applies both a constant confinement pressure and an axial load at a controlled rate to the coal sample and allows a given axial load to be maintained for an interval of time.

[5]Reference to specific products does not imply endorsement by the U.S. Bureau of Mines.

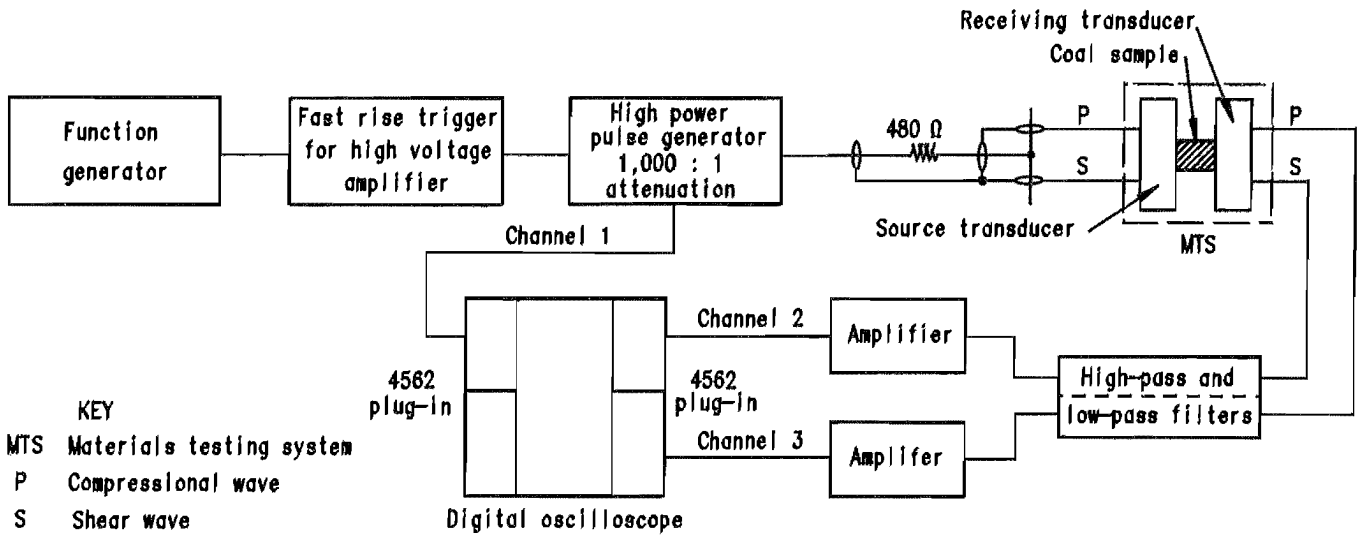

Figure 1.—Schematic diagram of experimental setup.

The transducers consist of lithium sulfate crystals that transmit and receive both P-waves and S-waves. Each transducer contains crystals generating P and S waves within one casing, with the P-wave crystal being annular, surrounding the central S-wave crystal. A correction factor must be included in attenuation calculations to compensate for signal attenuation caused by the transducers and coupling between the transducers and coal sample. The correction factor was determined by measuring the signal attenuation caused by the transducers themselves coupled together with no sample between. The Cober function generator is necessary to drive a large enough source signal through the coal sample. The signal voltage used for the test ranges from 500 to 600 V, and the frequency is 1 kHz. The pulse width of the driving signal from the Cober is 47 μs measured at 90% of average pulse amplitude, with 943 μs between pulses to allow for damping of all reflections in the sample before the next pulse arrives. The driving signal pulse excites simultaneously both the P-crystals and S-crystals in the driving transducer. Once the signals are input to the digital oscilloscope, the error involved in their measurement is $\pm$0.25 mV for amplitude and $\pm$0.25 μs for arrival time. The error involved in amplitude measurement leads to an error of $\pm$0.05 dB in P-wave attenuation values and an error of $\pm$0.03 dB in S-wave attenuation values (less than 0.1% error). The error involved in the arrival time measurement introduces an error of $\pm$42.6 ft/s into P-wave velocity values (approximately 0.5%) and $\pm$7.9 ft/s into S-wave velocity (approximately 0.2% error).

COAL SAMPLE PREPARATION

Large blocks of coal were obtained from three underground coal mines in Utah. Core samples were drilled from the blocks of coal using a water-cooled stationary laboratory drill and a diamond core barrel, 1.99 in. in inner diameter. The cores were oriented perpendicular to coal bedding. The core samples were then cut to the desired lengths using a water-cooled diamond blade masonry saw. Smooth surfaces at each end of the cores were necessary to provide adequate transducer coupling. The end surfaces of the cores were ground and polished with a precision surface grinder, which ensures parallelism between end surfaces within 0.001 in. Core samples were also tested for perpendicularity between the end surfaces and the core sides within 0.005 in to ensure that the transducers at each end are directed toward each other. After the samples were prepared, they were stored in sealed plastic tubes to preserve the moisture content of the coal. Thirty-one core samples were selected for testing. Each was weighed and measured before testing. The samples selected for triaxial testing ranged from 4.29 to 4.15 in. in length with the average being 4.19 in. The samples prepared for uniaxial tests were shorter (2.015 to 2.095 in) because it was difficult for the signal to travel through a longer, unconfined coal sample. A table of data on samples for which tests were completed successfully is included in table 1.

EXPERIMENTAL PROCEDURE

For each test, a coal sample was placed between 4-in long steel platens, 1.99 in. in diameter (fig. 2). A centered hole 0.6 in. in diameter within the platens contained the transducers and the spring-loads which pressed the transducers against the samples at a constant pressure. A steel disk the same diameter as the platens with the length of 0.70 in was attached to each platen by screws to hold the spring assembly in place. The coaxial cable that connected the source transducer to the function generator and receiving transducer to the oscilloscope passed through the center of the spring coil. A groove in the steel disk accommodated the cable (fig. 2). To assure good signal transmission between the coal sample and the transducers, a commercially available gel couplant designed for transmission of ultrasonic signals was applied to the transducers. Axial displacements were measured with linear variable differential transformers (LVDT's). For the uniaxial test, a three-ring holder LVDT was used. The bottom steel platen supported the base ring. The center ring held in place three LVDT's to measure the lateral displacement of the sample during vertical compression. The top ring held LVDT's that measured the axial displacement of the sample during vertical compression.

For triaxial tests the sample was surrounded by a neoprene sleeve to isolate it from hydraulic fluid, which was used to apply a uniform confinement pressure to the sample. The sample and sleeve were then placed in a steel triaxial chamber (fig. 3), 5 in. in outer diameter and 9.5 in. in length. For triaxial tests, only the top and bottom rings were used. These rings, supported by the steel platens, held in place three LVDT's to measure the axial displacement of the sample during vertical compression. No lateral measurements were possible during the triaxial tests. The confinement pressures used for triaxial testing included 250, 500, 750, 1,000, and 1,250 psi. Throughout the duration of each test, the confinement pressure was held constant within the triaxial load chamber.

Table 1.—Data on coal samples successfully tested

Coal seam and sample	Sample		Confinement pressure, psi	Load, lb	
	Length, in	Density, g/cm^3		At 1st signal received	At failure
Blind Canyon:					
Uniaxial 1	2.068	1.14	0	1,200	7,300
Uniaxial 2	2.015	1.13	0	0	7,700
Uniaxial 3	2.095	1.15	0	1,000	5,700
Uniaxial 4	1.932	1.15	0	0	13,350
Triaxial 1	4.185	1.26	250	1,000	14,200
Triaxial 2	4.188	1.36	250	1,000	11,400
Triaxial 3	4.180	1.17	500	2,000	21,400
Triaxial 4	4.158	1.32	500	4,000	18,600
Triaxial 5	4.187	1.28	750	0	20,150
Triaxial 6	4.191	1.32	1,000	0	29,000
Triaxial 7	4.291	1.22	1,000	4,000	23,400
Triaxial 8	4.233	1.22	1,250	4,000	30,450
Triaxial 9	4.195	1.60	1,250	1,000	24,600
Wattis Seam:					
Triaxial 10	4.210	1.38	250	0	17,700
Triaxial 11	4.165	1.39	500	0	20,750
Triaxial 12	4.214	1.38	500	0	19,250
Triaxial 13	4.193	1.44	750	0	20,200
Triaxial 14	4.183	1.38	750	4,000	19,250
Triaxial 15	4.173	1.44	750	0	14,550
Triaxial 16	4.168	1.29	1,000	4,000	20,900
Triaxial 17	4.196	1.38	1,250	4,000	28,200
Rock Canyon:					
Triaxial 18	4.215	1.30	250	2,000	15,900
Triaxial 19	4.210	1.28	250	4,000	14,850
Triaxial 20	4.155	1.29	500	4,000	23,000
Triaxial 21	4.170	1.30	750	1,000	23,550
Triaxial 22	4.233	1.31	1,000	0	27,300
Triaxial 23	4.165	1.29	1,000	1,000	32,100
Triaxial 24	4.168	1.29	1,250	0	33,950
Triaxial 25	4.193	1.30	1,250	0	28,150

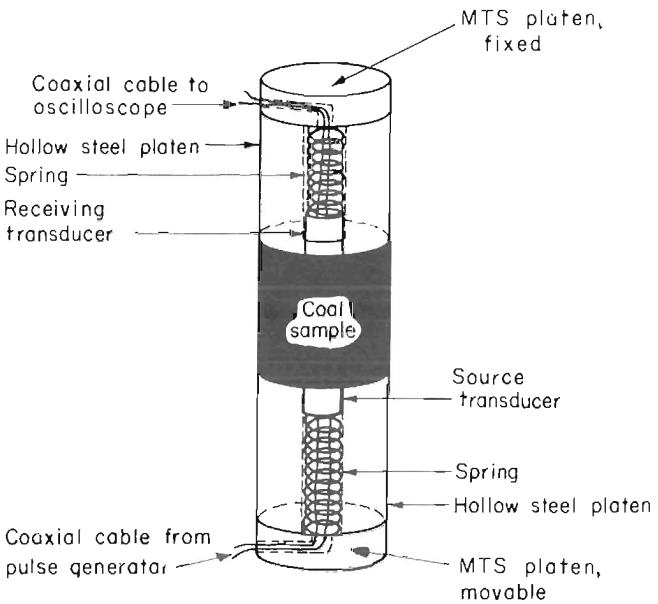

Figure 2.—Coal sample enclosed in steel platens with hollow internal chambers and enclosed springs to hold transducers against sample at constant pressure.

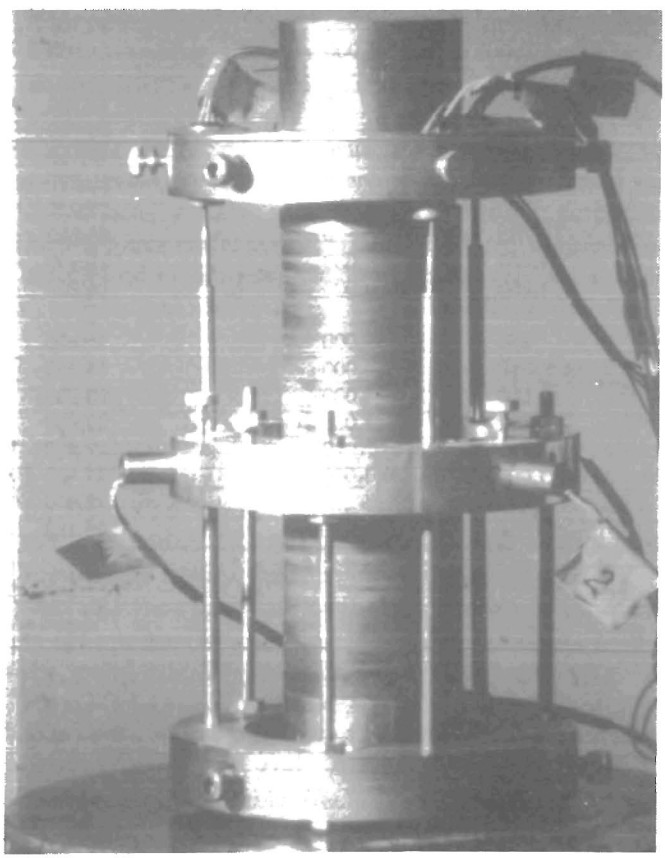

Figure 3.—Triaxial testing chamber within MTS platens.

The MTS applied an axial load to the sample by displacing the loading head at a fixed rate of 6.7×10^{-5} in/s. At axial load increments of 1,000 lb for the six uniaxial tests and 4,000 lb for the 25 triaxial tests, sample loading was suspended for 3 to 5 min after each increment to allow for structural stabilization within the sample in response to the increased load. At the end of each pause, while load was held constant, three arrival times and their corresponding maximum amplitudes were recorded and averaged for each wave type. Only four of the six uniaxial tests were successful. For the two unsuccessful tests, P-wave and S-wave signals were not able to be transmitted through the coal samples. Because of the layer cavities oriented parallel to bedding in the coal and perpendicular to signal propagation, P-wave and S-wave signals were not able to be transmitted through some of the coal samples at zero vertical load pressure. The load was applied until the sample could no longer support additional load, as determined by the MTS operator. At this point, the sample was considered to have structurally failed. After sample failure, while the load was removed from the sample, arrival times and amplitude measurements were recorded when there was adequate signal reception through the coal. In a few of the triaxial tests, no signals could be transmitted through the failed sample. During only one uniaxial test were any postfailure measurements possible.

Control of postfailure sample unloading was difficult to maintain. For this reason postfailure data readings were taken at random values of load. Because the sample was failed, it was difficult to maintain a fixed load long enough to take more than one arrival time and amplitude reading for each load.

A plotter attached to the MTS continuously recorded change in sample length versus applied load. The MTS measured the applied load, while the LVDT's measured change in sample length. From the sample lengths and the travel times measured at each load point, the velocities of the S-waves and the P-waves were calculated. Axial deformation, in response to loading of the sample, was included in each velocity calculation. Attenuation of the signals caused by travel through the coal sample was calculated by comparing the amplitudes of the input and output signals, as shown in the equation,

$$\text{Attenuation} = 20 \log (\text{output voltage}/\text{input voltage}).$$

To compare attenuation values between samples of different lengths, the attenuation coefficient was also calculated using the equation,

$$I_x = I[(e^{-ax})/x],$$

where a = the attenuation coefficient,

I = initial amplitude,

and I_x = amplitude at distance x from the source (*15*).

Ratios of P-wave velocity to S-wave velocity were calculated. The velocity values were normalized by the initial velocity values to evaluate percent change of velocity with each loading increment. All the parameters were plotted and evaluated to determine whether any trends existed in response to sample loading and failure.

DISCUSSION OF RESULTS

VELOCITY AND ATTENUATION

Figures 4 and 5 show representative trends of velocities and signal attenuation values for P-waves and S-waves, respectively, from a uniaxial test. Figures 6 and 7 show trends for the P-waves and S-waves, respectively, from a representative triaxial test, confinement pressure of 250 psi. The graphs for the remaining samples are included in the appendix. As the initial load is applied to the coal sample, there is a high rate of increase in velocity and decrease in attenuation, which is labeled phase 1. This phase signifies the closing of layer cavities in the coal sample by the initial load, thus allowing the signals to travel more efficiently through the coal with greater velocity and less attenuation. The decline in rate of velocity increase, and attenuation decrease is labeled phase 2, and indicates that the closing of layer cavities within the coal samples is complete. The linear increase of velocity with respect to increase in load reflects the increase in density caused by elastic compaction of the sample with applied load.

In phase 3, the applied load, instead of closing microfractures, appears to be creating microfractures within the coal sample. The presence of microfractures causes an increase in attenuation, which is more sensitive to their presence. However, velocity remains fairly constant or increases slightly. Although the microfractures may be developing, they do not impair the ability of the sample to bear load or decrease the velocity of elastic waves travelling through the sample. The change in attenuation behavior, without a corresponding change in velocity behavior, indicates that this phase is a transitional one signifying the first stages of failure. The sample is not considered to be failed until it can no longer bear an increase in load or maintain a fixed load. At failure, the changes in velocity and attenuation are abrupt (figs. 4-5).

In general, the P-wave curves do not demonstrate the described phases as consistently as the S-wave curves. The phases are discernible in the uniaxial and triaxial P-wave graphs in figures 4 and 6, but were not so clear in the majority of the P-waves. The increases in the P-wave velocity with load increase was probably masked by the sampling interval of the oscilloscope (0.5 μs), which, as discussed earlier, would not detect changes in the P-wave velocity of less than 42.6 ft/s, but would detect changes in the S-wave velocity greater than 7.9 ft/s. At zero load, approximately half the samples did not allow transmission of P-waves or S-waves (table 1). An initial load of 1,000 to 4,000 lb was required before measurable waveforms were transmitted through the sample. For samples subjected to confining pressures, a greater initial axial load had to be applied before a signal could penetrate the coal sample. The effect may have been caused by the fact that confinement pressure, which is applied laterally to the sample and parallel to the layer cavities, acted to hold the layer cavities open during the lower load values. Once a large enough axial load was applied, the effect of confining pressure was offset sufficiently to allow closure of the layer cavities. The signals could then be transmitted through the sample.

Confining pressure also affects the boundaries of the phases 2 and 3 for the coal samples. The phase boundaries, as defined by load increments, were averaged for each confining pressure group. In general, as confining pressure increased, the load increments defining the boundaries for phases 2 and 3 increased. The average load at ultimate sample failure also increased with confining pressure.

MODE OF FAILURE

According to Paterson (*16*), the physical behavior of coal samples loaded axially to failure can be described by three stages. Stage 1 begins with the initial application of load, during which the deformation is nonlinearly elastic with respect to load. The behavior is due to the closure of preexisting voids within the coal parallel to bedding. Stage 1 corresponds to phase 1 as defined by the behavior of wave attenuation and velocity. Stage 2 begins after the layer cavities within the sample have closed, and elastic deformation behaves linearly with respect to load. Stage 2 corresponds to phase 2 as defined with velocity and attenuation measurements. Stage 3 (fig. 6) begins with the development of microfractures throughout the sample. These microfractures are oriented parallel to the direction of axial loading. The microfractures cause

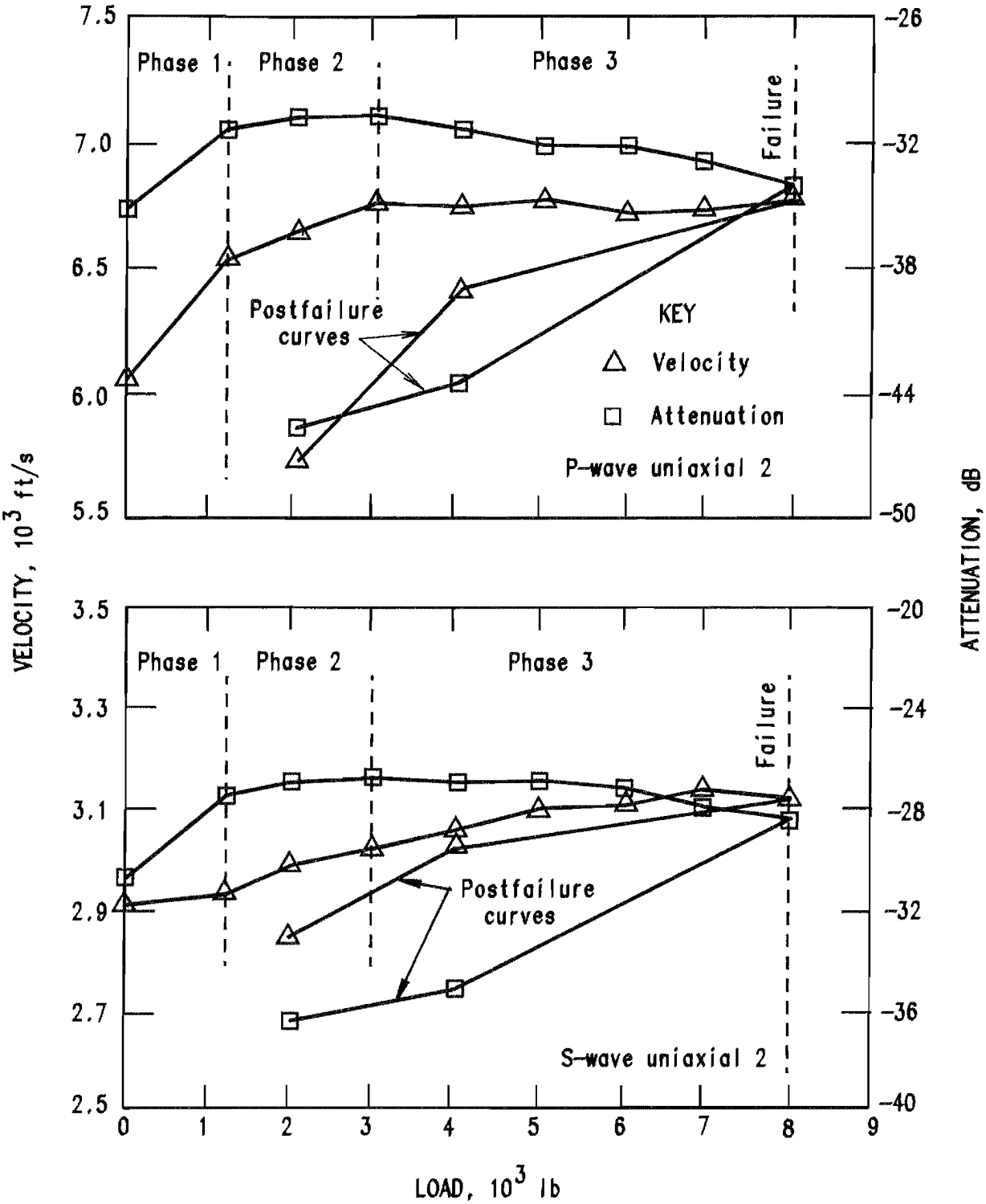

Figure 4.—Velocity and attenuation of waves versus load for uniaxial test, showing the three phases of behavior change as load increases and as failure occurs.

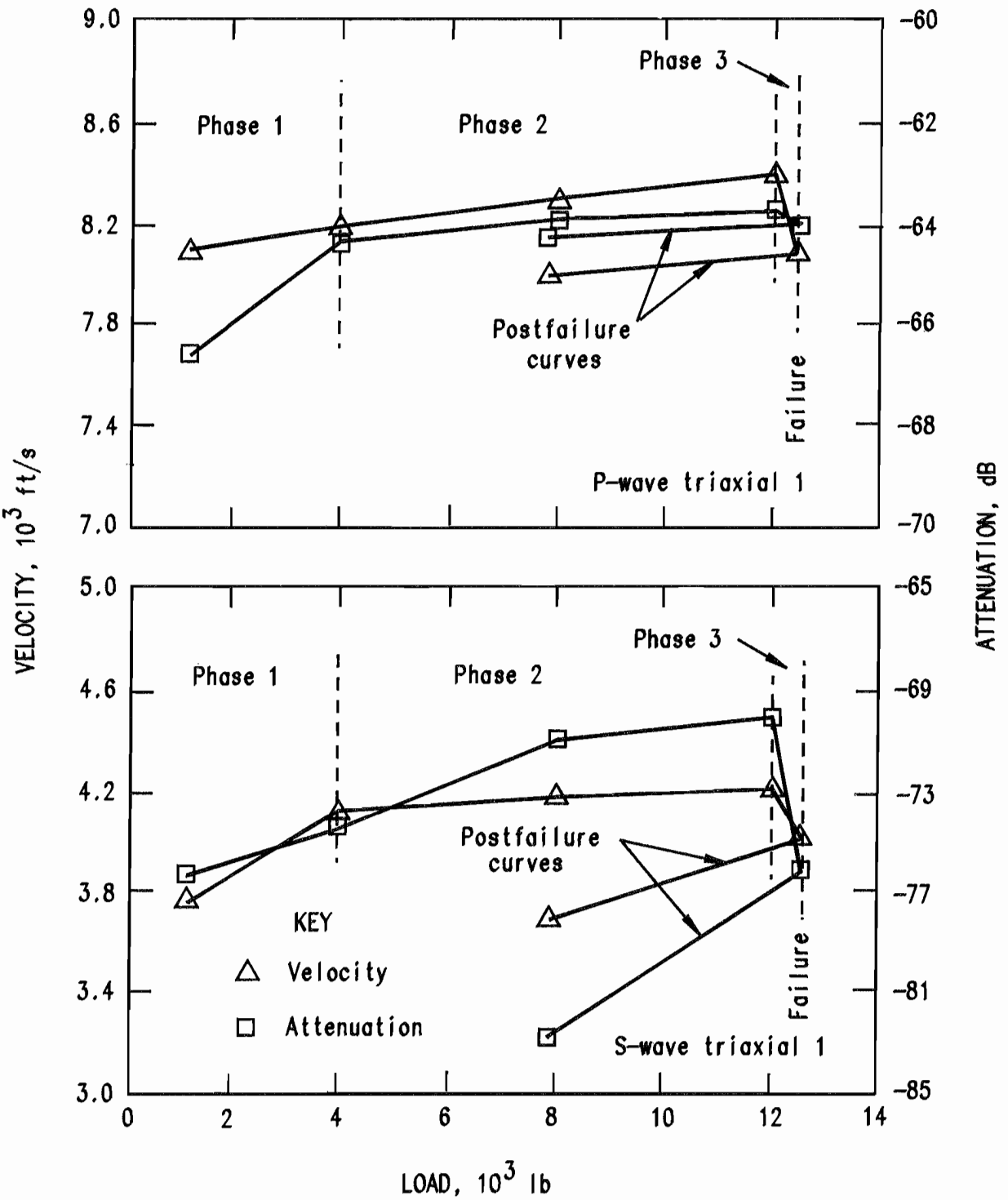

Figure 5.—Velocity and attenuation of waves versus load for triaxial test, showing the three phases of behavior change as load increases and as failure occurs.

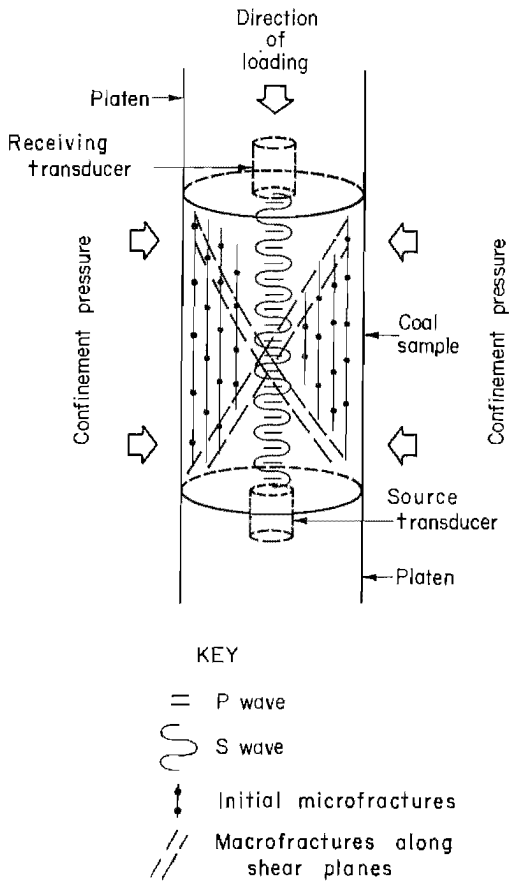

Figure 6.—Illustration of mode of failure for coal sample subjected to axial loading.

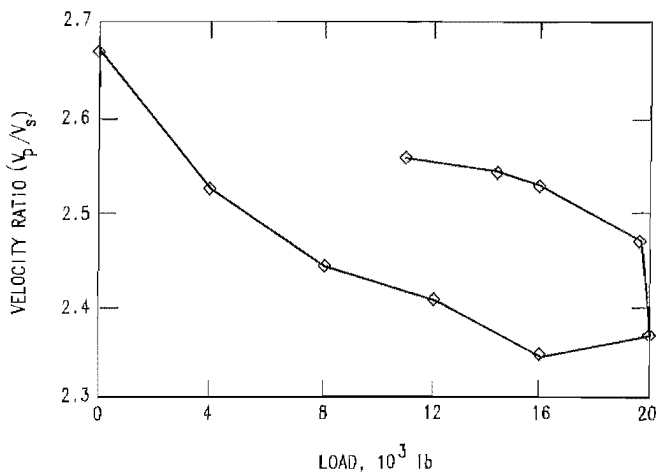

Figure 7.—Ratios of P-wave velocity to S-wave velocity versus load.

an increase in attenuation, which is more sensitive than velocity to their presence. Phase 3 is thought to end when microfracture development within the sample causes a decrease in velocity. Stage 3 ends when microfractures coalesce to form macrofractures, which concentrate along shear planes and lead to sample failure (*11-12, 17*). At this point, there is an abrupt increase in attenuation and decrease in velocity (figs. 4-5).

VELOCITY RATIOS (V_p/V_s)

Because the S-wave is more responsive than the P-wave, the expected trends occur consistently in the plots of velocity ratios. Figure 7 shows a typical plot of the ratio of the P-wave velocity (V_p) to the S-wave velocity (V_s) during loading and after failure. The plot is of triaxial sample 14 with confinement pressure of 500 psi. Initially the ratio decreases as the S-wave velocity increases at a faster rate than the P-wave velocity, corresponding to phase 1 on the velocity-attenuation curves. Once the load closes the layer cavities within the sample, both P-wave and S-wave velocities stabilize, as indicated by a flattening of the ratio curve. This portion of the curve corresponds to phases 2 and 3 of the velocity-attenuation curves, but the behavior of the velocity ratio illustrates no clear division between the two phases. Then upon failure, a sudden rise in the ratio shows that the S-wave velocity decreases at a greater rate than the P-wave velocity.

ATTENUATION RATIOS (A_p/A_s)

The ratios of P-wave attenuation (A_p) to S-wave attenuation (A_s) also consistently demonstrate the expected trends. Figure 8 shows an example of the typical attenuation ratio plot. The plot is of triaxial sample 10 with confinement of 750 psi. The ratio increases upon initial loading, as the S-wave attenuation becomes smaller with crack closure, corresponding to phase 1 on the velocity-attenuation curves. The attenuation curve then flattens, corresponding with phases 2 and 3 of the velocity-attenuation curves, with no clear division between the two phases. Attenuation ratio decreases upon failure as resulting fractures increase S-wave attenuation significantly.

DYNAMIC ELASTIC CONSTANTS

The dynamic elastic constants were calculated from the P-wave and S-wave velocities according to the following equations:

$$\text{Poisson's ratio} = [1/2 - (Vs/Vp)^2] / [1 - (Vs/Vp)^2] = \nu,$$

$$\text{Shear modulus} = \rho Vs^2,$$

$$\text{Bulk modulus} = \rho[Vp^2 - (4/3)Vs^2],$$

$$\text{Young's modulus} = Vp^2\,\rho[(1 - 2\nu)(1 + \nu) / (1 - \nu)],$$

where Vp = P-wave velocity,

Vs = S-wave velocity,

ρ = pretesting density of coal sample,

and ν = Poisson's ratio (*18*).

Three of the dynamic elastic constants behaved consistently, but the fourth, the bulk modulus, showed no consistency from one sample test to another. The graphs shown in figures 9 and 10 represent dynamic elastic constant values calculated from the elastic wave velocities measured for sample 22 with confinement pressure of 1,250 psi.

Figure 9 shows a typical example of Poisson's ratio versus load. The ratio decreases initially, indicating that lateral deformation of the sample is increasing relative to the corresponding axial deformation. If initial loading of the sample serves only to close the layer cavities in the coal, causing axial deformation, it would be accompanied by minimal lateral deformation. Additional loading would close fewer layer cavities, as fewer would remain open with increased loading. Thus, additional axial shortening would result in increasing lateral expansion, decreasing Poisson's ratio. The curve flattens at the intermediate loads, indicating that axial shortening and lateral expansion may be occurring elastically with minimal influence from fractures. This portion of the curve coincides with phases 2 and 3 on the velocity-attenuation curves. Upon failure of the sample, Poisson's ratio increases, indicating relative increase in lateral deformation.

Figure 10 shows the shear modulus and Young's modulus versus load. These two moduli consistently show similar behavior patterns for each sample test, even though the shear modulus describes shear deformation and its value depends only on the S-wave velocity, while Young's modulus describes the shortening of the sample and its value depends on the P-wave velocity and Poisson's ratio. At points of initial loading (phase 1), the values of these moduli increase. This behavior suggests that with initial loading, the change in stress and strain is nonlinear, responding to the closing of the layer cavities within the coal. Once the layer cavities are closed, the curve flattens at the intermediate loads (phases 2 and 3), suggesting that stress and strain are changing linearly with each load. Upon sample failure, the values for each modulus decrease, as the resulting strain increases greatly compared with the stress.

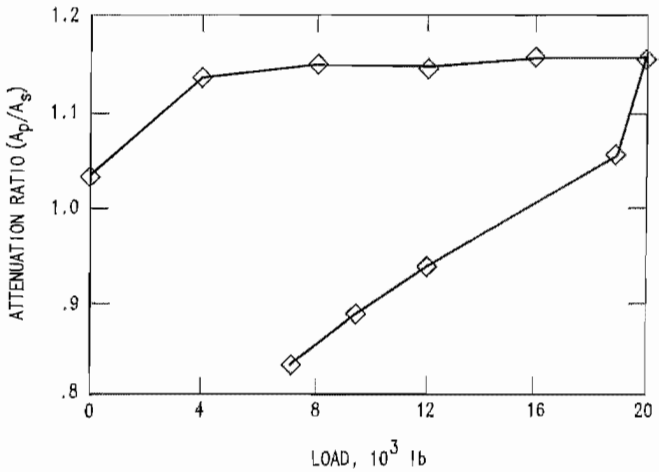

Figure 8.—Ratios of P-wave attenuation to S-wave attenuation versus load.

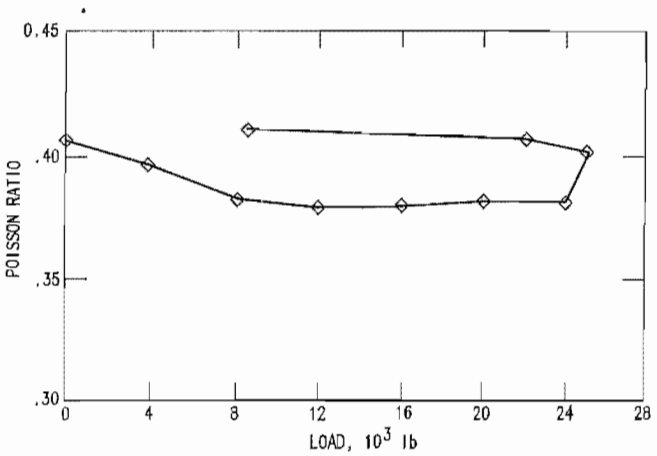

Figure 9.—Poisson's ratio of coal versus load.

Figure 10 also shows the bulk modulus, which is a measure of volume change with loading. The bulk modulus demonstrated inconsistent trends for the sample tests. Under initial sample loading, approximately half the samples showed increasing bulk modulus values, while the other half of the samples showed decreasing values. For 12 samples, the bulk modulus increased in value just before failure, for six samples bulk modulus decreased in value, while nine samples showed unchanging values, indicated by flat curves. Upon sample failure, the bulk modulus of half the samples increased, while the other half showed decreasing values. The variation in behavior of the bulk modulus from sample to sample may be a consequence of the nature of coal itself. Coal has many physical and compositional discontinuities, such as layer

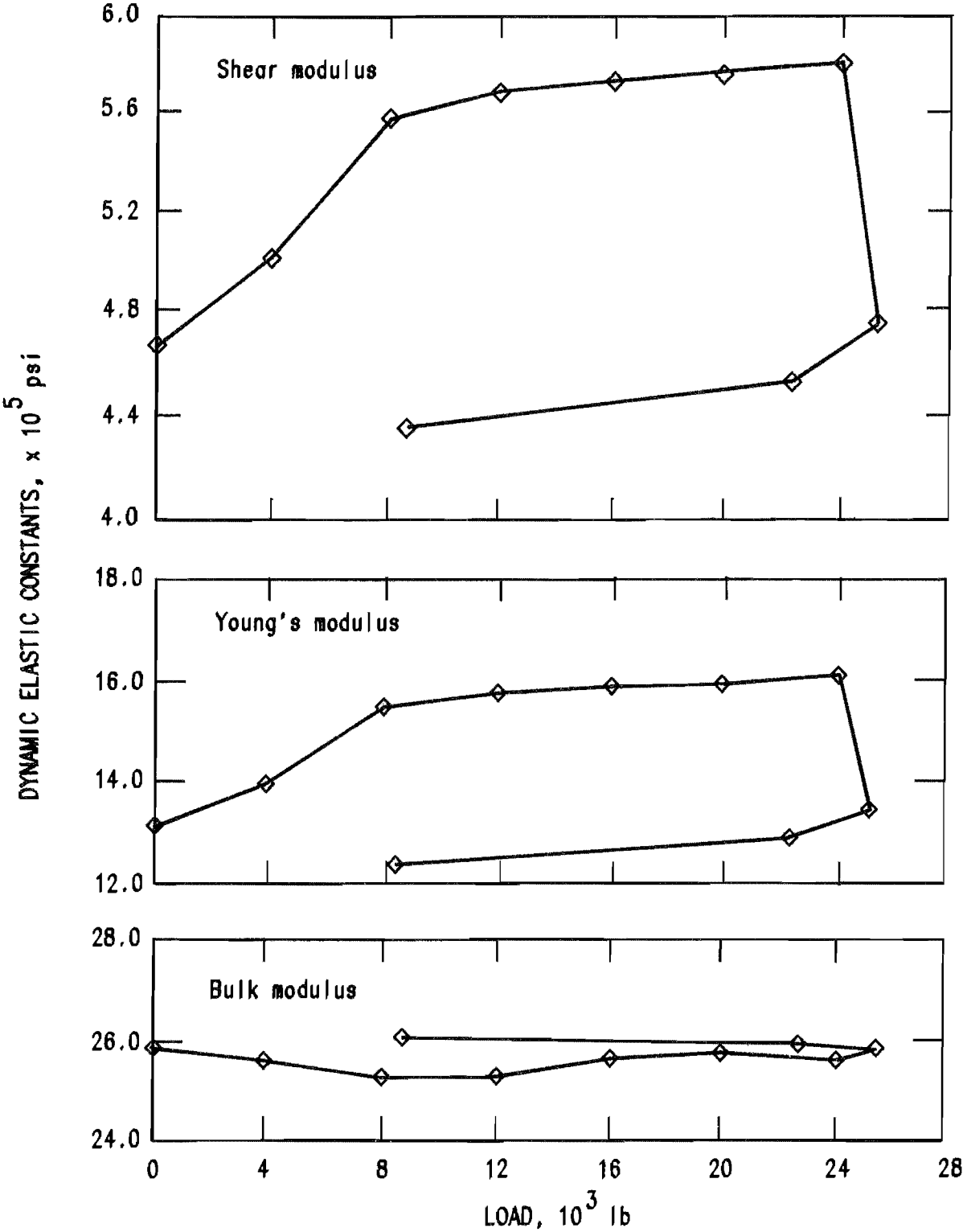

Figure 10.—Shear modulus, Young modulus, and bulk modulus versus load.

cavities and cleat and a number of very brittle components, which cause each sample to demonstrate different patterns of dilatant behavior upon loading and failure. As a result, the dilatancy of coal is not as predictable as its other deformational properties. Another factor could be the inability to measure the change in sample density during triaxial loading. The trends of the bulk modulus may be more sensitive to the changing density than the trends of the other dynamic elastic moduli.

Because the dynamic elastic constants are calculated from the elastic wave velocities, they do not exhibit the same degree sensitivity as attenuation to the phases of loading and microfracture development. As a whole Poisson's ratio, Young's modulus, and the shear modulus show consistent behavior patterns upon loading and failure, but they are not helpful in defining the subtle phases previously discussed for velocity and attenuation. The behavior of dynamic elastic constants in response to fracture formation in rock samples is discussed by Zimmerman (*19*). He states that the presence of very small fractures in brittle material lowers the elastic moduli. For this series of tests of coal samples this statement holds true for the shear modulus and for Young's modulus. As the layer cavities are closed and their effects on these two moduli are diminished, the values of the moduli increase. Upon sample failure and associated fracture development, the moduli values decrease. However, Poisson's ratio decreases upon crack closure, and increases upon fracture development at failure. No conclusions can be drawn for the bulk modulus, based on these experimental results.

ATTENUATION COEFFICIENTS AND NORMALIZED VELOCITY

The attenuation coefficient curve (fig. 11) is a mirror image of the original attenuation curve with the X-axis as the axis of symmetry. Therefore, the trends illustrated by the original attenuation curve appear in the attenuation coefficient curve, but in inverse form. The points at which attenuation increases, the attenuation coefficient decreases, and conversely, where attenuation decreases, the attenuation coefficient increases.

Velocity values, normalized by the values of velocity at minimum load (fig. 12), illustrate a percent change of velocity with each load increment. Approximately the same trends observable in the original velocity curves are exhibited in the normalized velocity curves. There is a rapid increase in the normalized velocity values upon initial sample loading, rapid decrease of normalized values upon failure, and a flattening of the normalized velocity curve after initial loading and before failure.

CONCLUSIONS

The results of these experiments performed on coal core samples show that S-wave velocity and attenuation are the best parameters of those investigated to distinguish phases of loading and the onset of failure. The dynamic elastic constants, except the bulk modulus, and A_p/A_s and V_p/V_s ratios are valuable only to distinguish the early closure of layer cavities and failure of the sample, but do not appear to be sensitive to changes in load after crack closure. Attenuation coefficients and normalized velocity values reflect trends illustrated more simply by the original velocity and attenuation curves. It is important to compare the changes in behavior of velocity and attenuation together in response to loading and failure, so that the previously described phases may be distinguished. Phase 3 is significant in that it appears to be a phase of structural degradation within the sample that is a precursor to ultimate failure. Molina (*13*) correlated the timing of crack propagation that accompanies failure with reaching the maximum stress level with which the sample can be loaded. However, phase 3 occurs before the maximum stress is attained, indicating that microfractures begin to form earlier than the testing methods of Molina were able to detect. Observation of both attenuation and velocity changes is necessary to detect this phase. Phase 3 might correspond to the zone adjacent to the interior boundary of the yielded zone of a coal pillar where confinement pressures hold in place material exhibiting incipient fracturing.

The results discussed in this report, supported by the results of previous research in this field, indicate that P wave and S-wave attenuation and velocity should be effective in detecting the extent of the yield zone and the stress abutment peak within a coal pillar. Based on laboratory results, probably no signal will be transmittable through the failed material of the yield zone. The yield zone will probably be detectable by the transmission of the signal through the coal within the pillar. The P-wave and S-wave velocities and attenuation should then indicate an increase in stress on the coal within the pillar until the stress abutment peak, stress values should decrease, with the decrease being detectable by the change in signal velocity and attenuation. The next step is to test the technique in the field to verify its effectiveness.

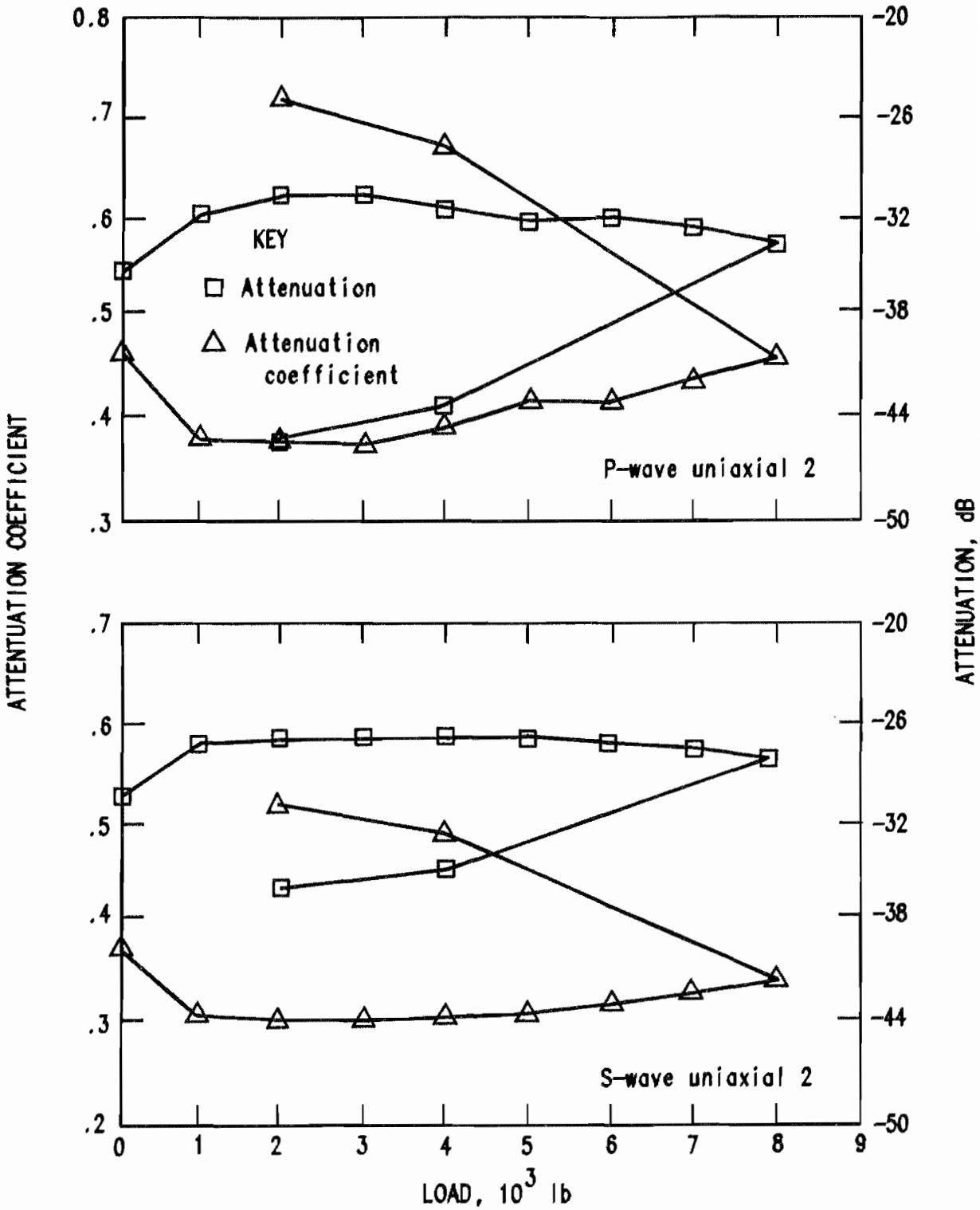

Figure 11.—Attenuation coefficient and attenuation versus load.

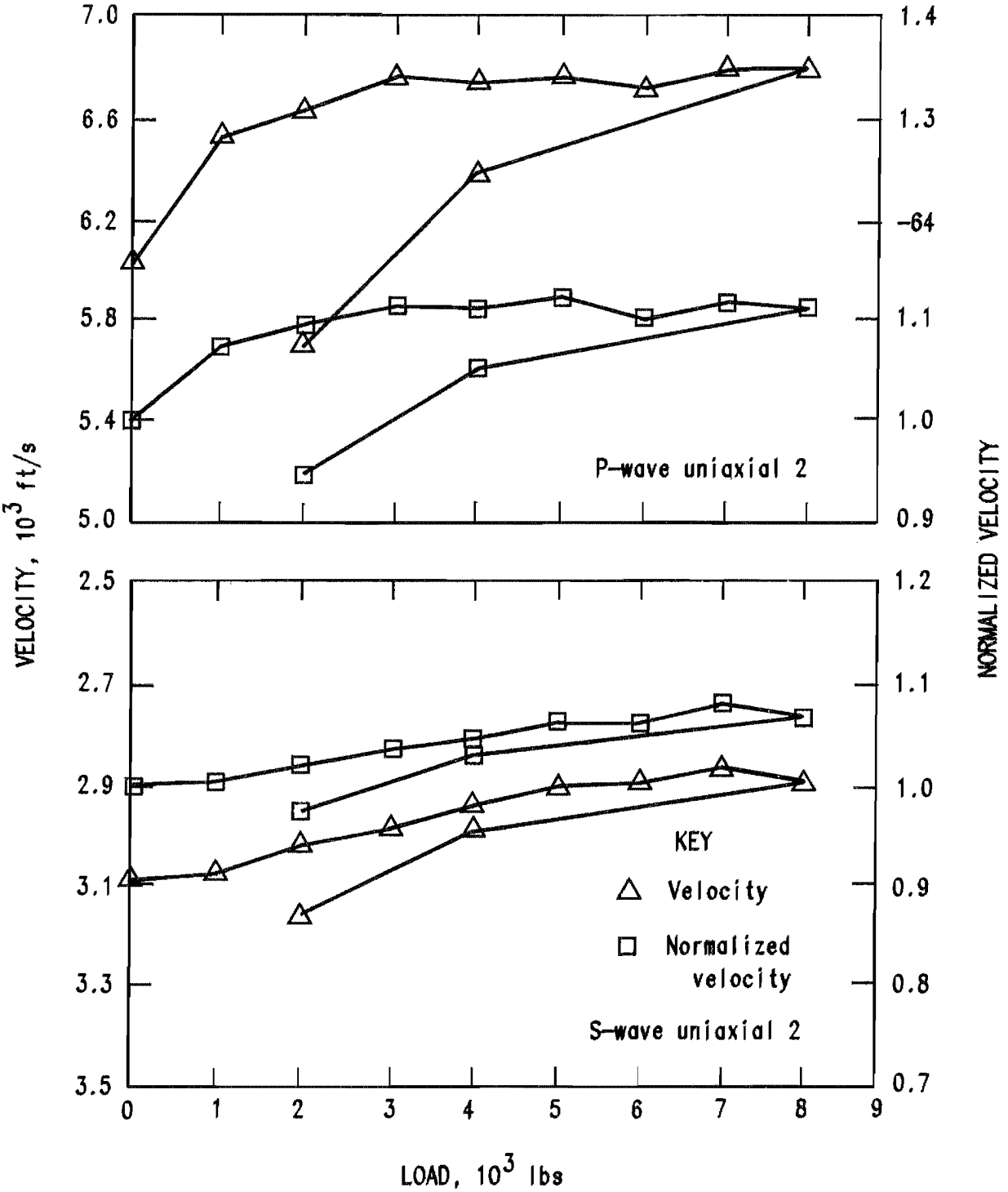

Figure 12.—Normalized velocity and velocity versus load.

REFERENCES

1. Wilson, W. H. Research Into the Determination of Pillar Sizes: Part I—An Hypothesis Concerning Pillar Stability. Min. Eng., v. 131, 1972, pp. 409-417.

2. ____. The Effect of Yield Zones on the Control of Ground. Paper in Proceedings of Sixth International Strata Control Conference (Banff, Canada, Sept. 23-28, 1971). CANMET and Can. Inst. Min. Metall., 1977, pp. 1-21.

3. ____. Stress and Stability in Coal Ribsides. Paper in Proceedings First Conference on Ground Control in Mining (Morgantown, WV, July 27-29, 1981). WV Univ., Morgantown, WV, 1981, pp. 1-12.

4. Tatham, R. H. Vp/Vs and Lithology. Geophysics, v. 40, 1982, pp. 336-344.

5. Hajnal, Z., M. R. Stauffer, M. S. King, P. F. Wallis, H. F. Wang, and L. E. A. Jones. Seismic Characteristics of a Precambrian Pluton and Its Adjacent Rocks. Geophysics, v. 40, 1983, pp. 569-581.

6. Su, W. H., S. S. Peng, S. Okuba, and K. Matsuki. Development of Ultrasonic Methods for Measuring In Situ Stresses at Great Depth. Min. Sci. Technol., v. 1, 1983, pp. 21-42.

7. Gladwin, M. T. Ultrasonic Stress Monitoring in Underground Mining. Int. J. Rock Mech. Min. Sci. & Geomech. Abstr., v. 19, 1982, pp. 221-227.

8. McKenzie, C. K., G. P. Stacey, and M. T. Gladwin. Ultrasonic Characteristics of a Rock Mass. Int. J. Rock Mech. Min. Sci. & Geomech. Abstr., v. 19, 1982, pp. 25-30.

9. Lin, P., and G. A. Faulkner. A Sonic Wave Attenuation Technique for Monitoring Stress Levels. Paper in Proceedings Fourth Conference on Ground Control in Mining (Morgantown, WV, July 22-24, 1985). WV Univ., Morgantown, WV, 1985, pp. 196-205.

10. Stacy, T. R. Seismic Assessment of Rock Masses. Paper in Proceedings Symposium on Exploration for Rock Engineering (Johannesburg, Nov. 1-5, 1976). South Afr. Div. Civ. Eng., Geotech. Div., Johannesburg, 1976, pp. 113-117.

11. Lockner, D. A., J. B. Walsh, and J. D. Byerlee. Changes in Seismic Velocity and Attenuation during Deformation of Granite. J. Geophys. Res., v. 82, 1977, pp. 5374-5377.

12. Thill, R. E. Acoustic Methods for Monitoring Failure in Rock. Proceedings 14th Symposium on Rock Mechanics. (University Park, PA, June 11-14, 1972). Am. Soc. Civ. Eng., New York, 1973, pp. 649-687.

13. Molina, J. P., and B. Wack. Crack Field Characterization. Int. J. Rock Mech. Min. Sci. & Geomech. Abstr., v. 19, 1982, pp. 267-278.

14. Terry, N. B. Dependence of Elastic Behavior of Coal on Microcrack Structure. Fuel, v. 3, 1959, pp. 125-146.

15. Dobrin, M. B. Introduction to Geophysical Prospecting, McGraw-Hill, NY, 1976, 630 pp.

16. Paterson, M. S. Experimental Rock Deformation—The Brittle Field. Springer-Verlag, NY, 1978, 254 pp.

17. Elliot, G. M., and E. T. Brown. Yield of a Soft, High Porosity Rock. Geotechnique, v. 35, 1985, pp. 413-423.

18. Duvall, W. I. The Effect of Anisotropy on the Determination of Dynamic Elastic Constants of Rocks. Trans. Soc. Min. Eng., v. 232, 1965, pp. 309-316.

19. Zimmerman, R. W. The Effect of Microcracks on the Elastic Moduli of Brittle Materials. J. Mater. Sci. Letters, v. 4, 1985, pp. 1457-1460.

APPENDIX.—VELOCITY AND ATTENUATION OF WAVES VERSUS LOAD FOR UNIAXIAL AND TRIAXIAL TEST SAMPLES

The figures contained in the appendix show the velocity and attenuation of P-wave and S-wave signals versus load for the uniaxial and triaxial tests not specifically discussed in the main text. The velocity values are on the left vertical axis and the attenuation values are on the right vertical axis. The confinement pressures at which each sample was tested are included in table 1.

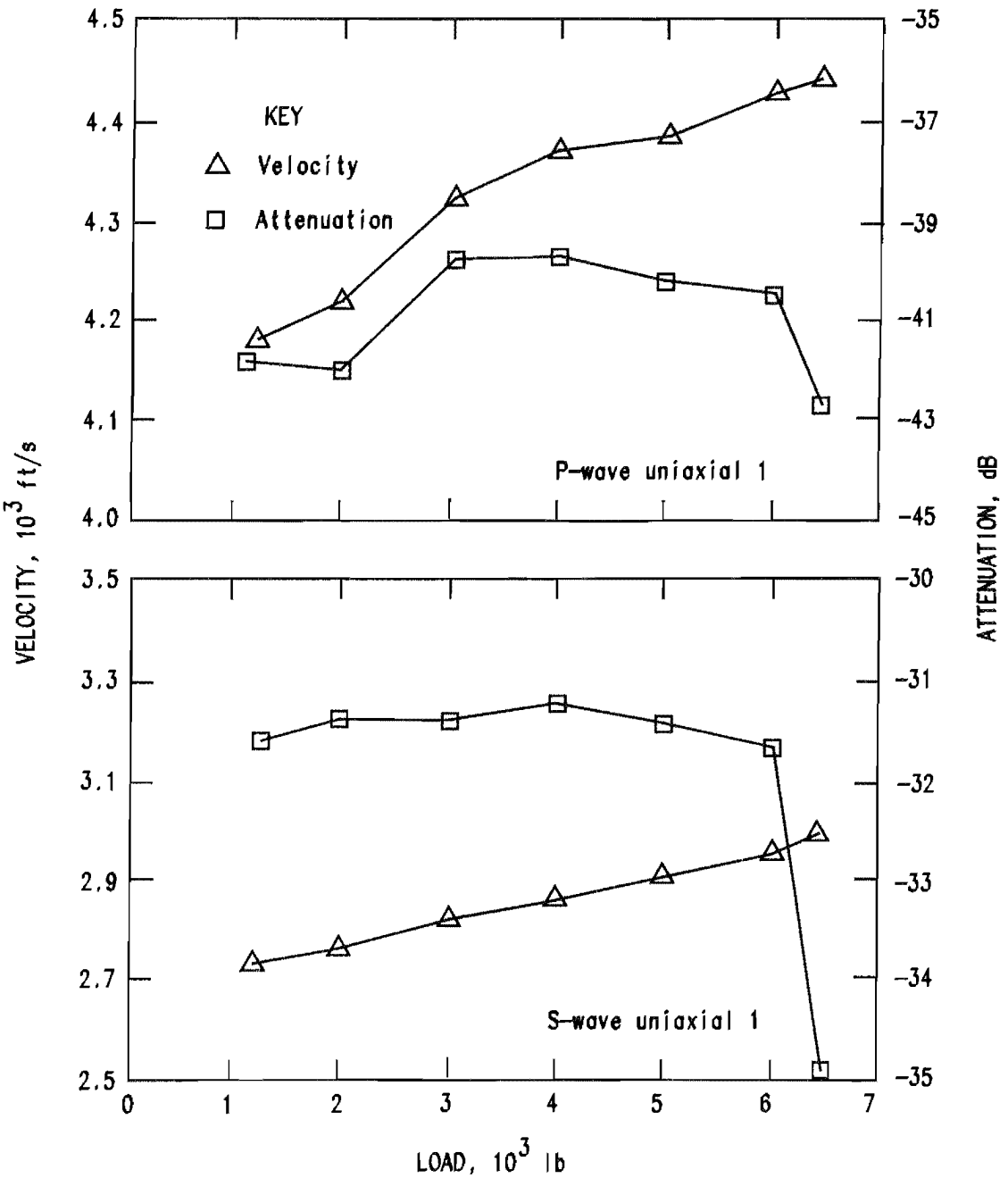

Figure A-1.—Velocity and attenuation of waves versus load for uniaxial test 1, showing the three phases of behavior change as load increases and as failure occurs.

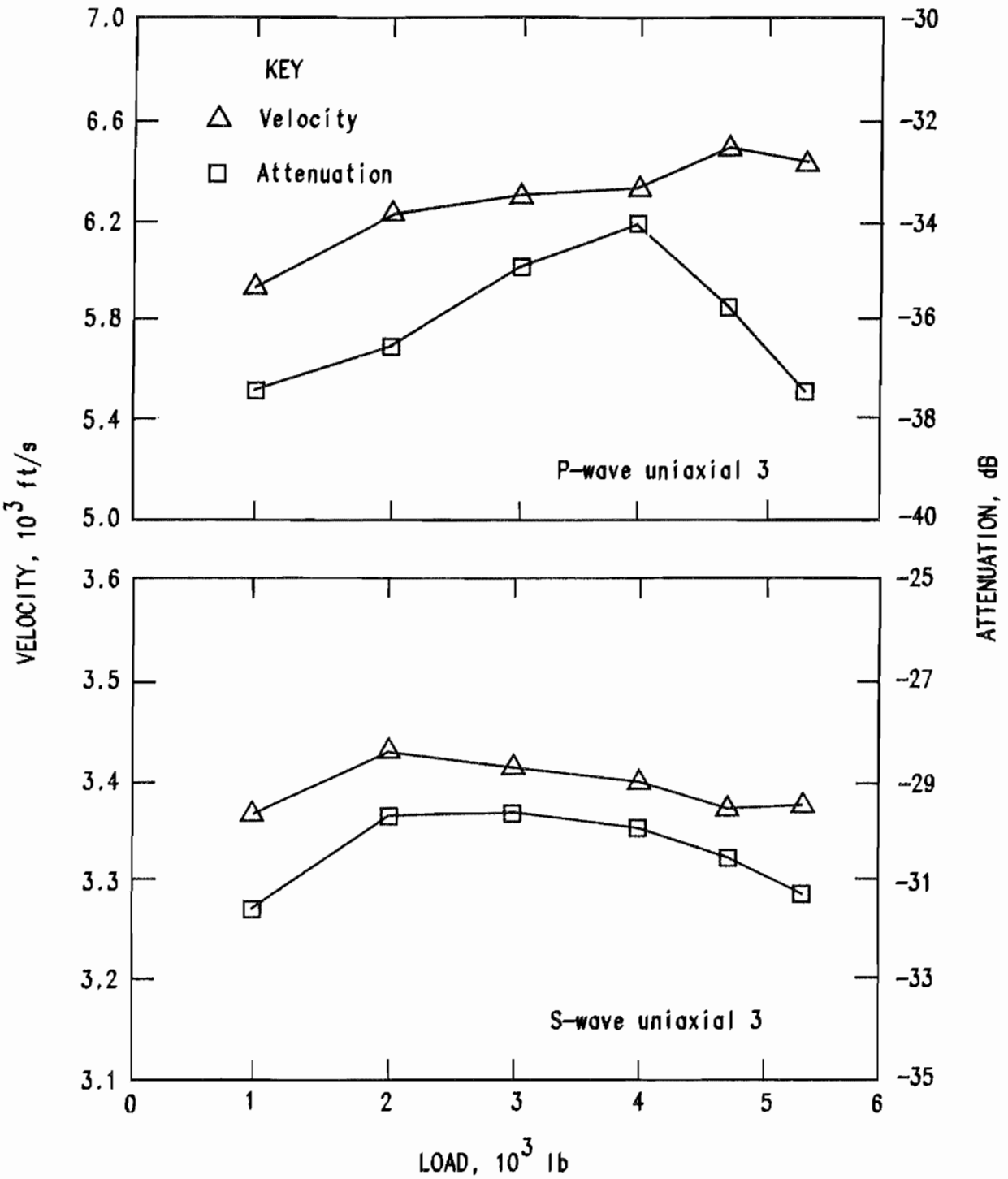

Figure A-2.—Velocity and attenuation of waves versus load for uniaxial test 3, showing the three phases of behavior change as load increases and as failure occurs.

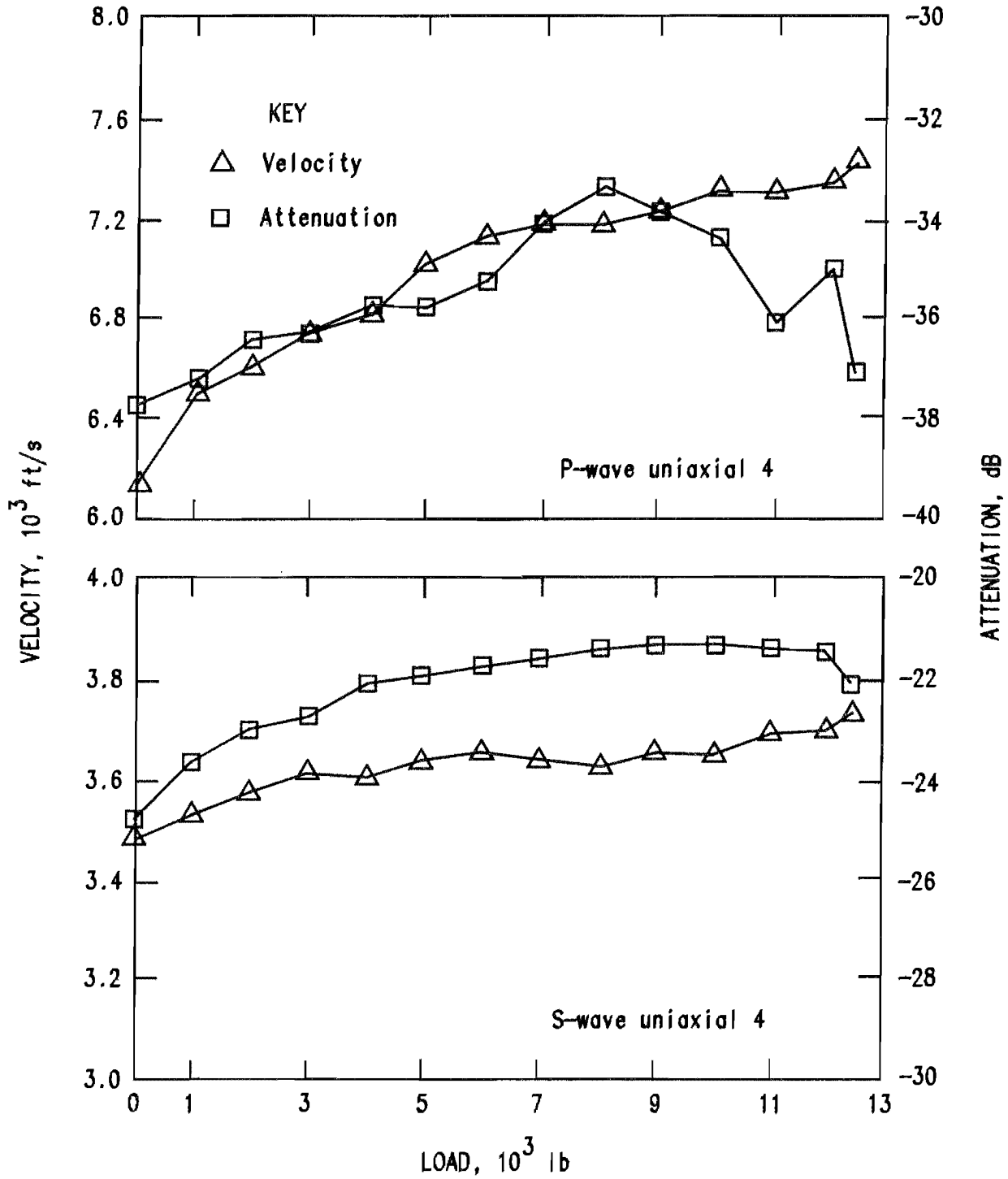

Figure A-3.—Velocity and attenuation of waves versus load for uniaxial test 4, showing the three phases of behavior change as load increases and as failure occurs.

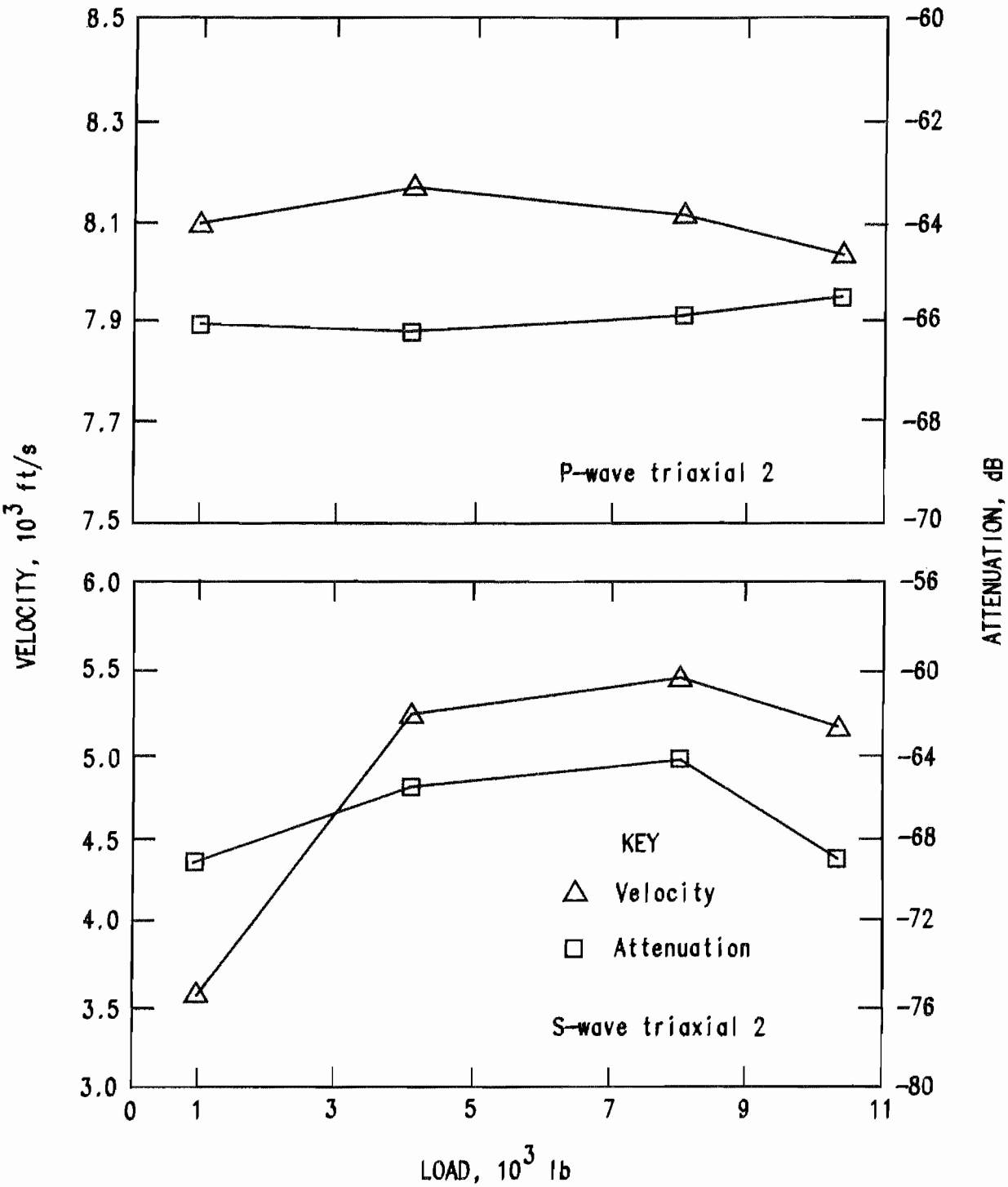

Figure A-4.—Velocity and attenuation of waves versus load for triaxial test 2, showing the three phases of behavior change as load increases and as failure occurs.

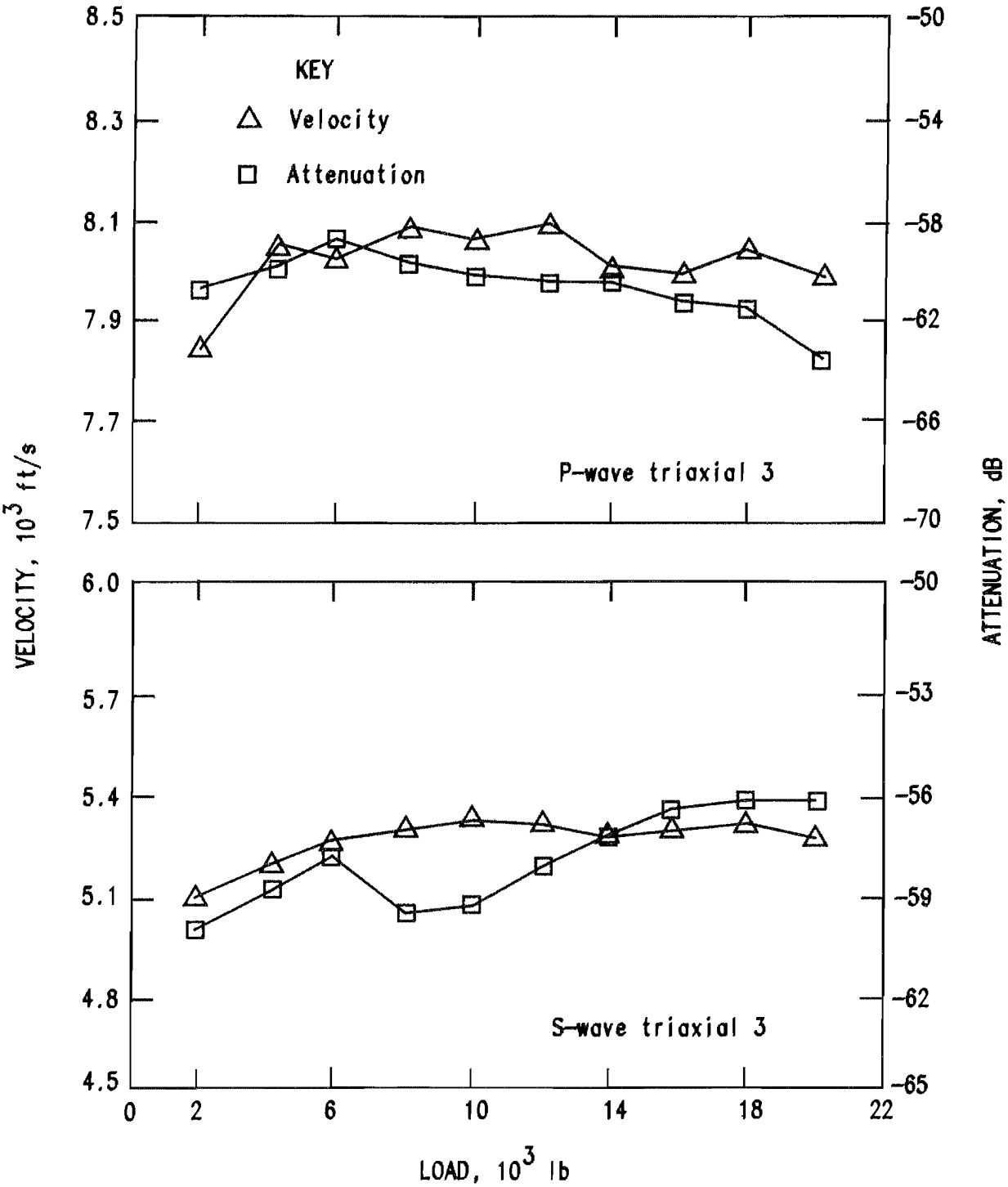

Figure A-5.—Velocity and attenuation of waves versus load for triaxial test 3, showing the three phases of behavior change as load increases and as failure occurs.

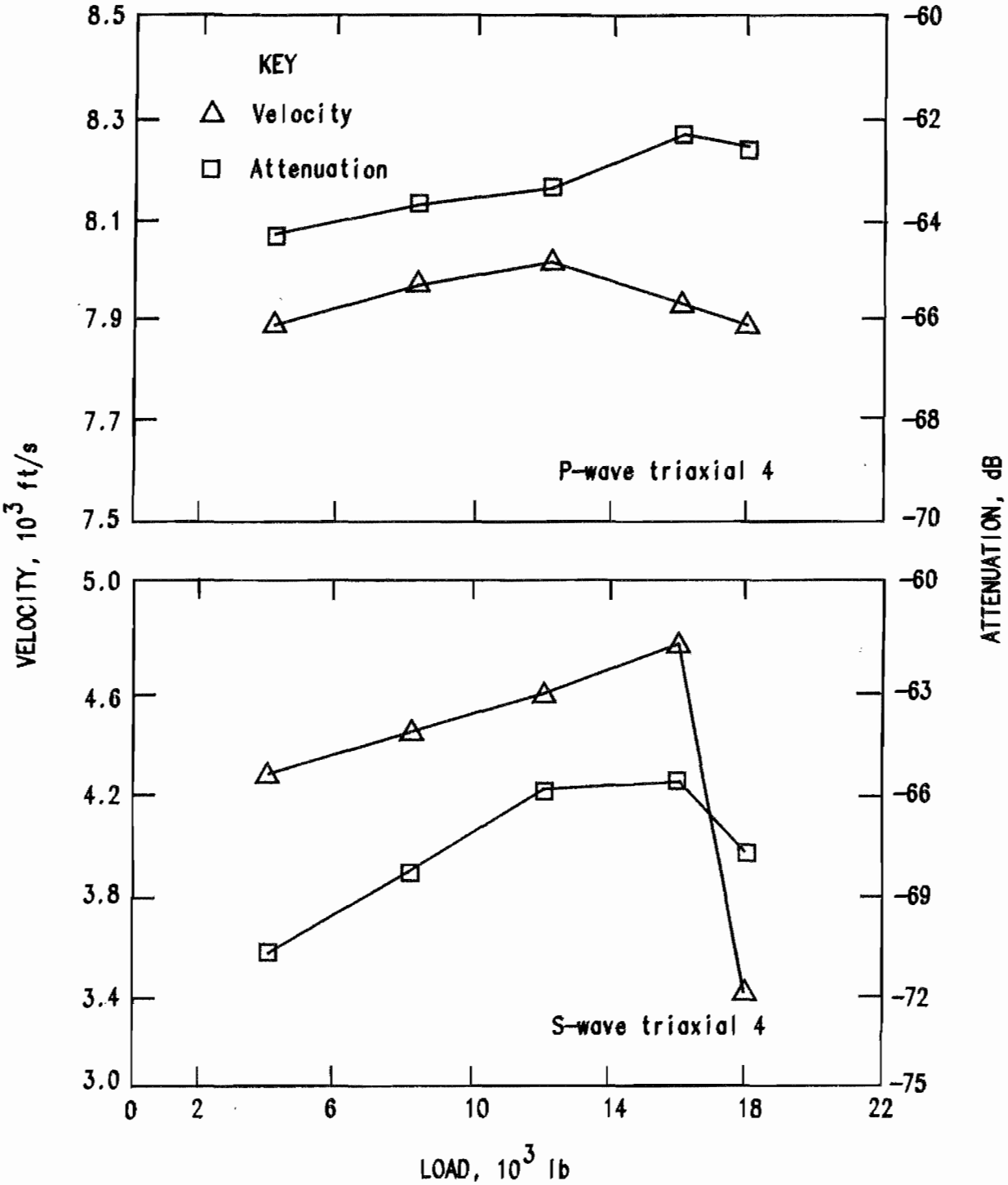

Figure A-6.—Velocity and attenuation of waves versus load for triaxial test 4, showing the three phases of behavior change as load increases and as failure occurs.

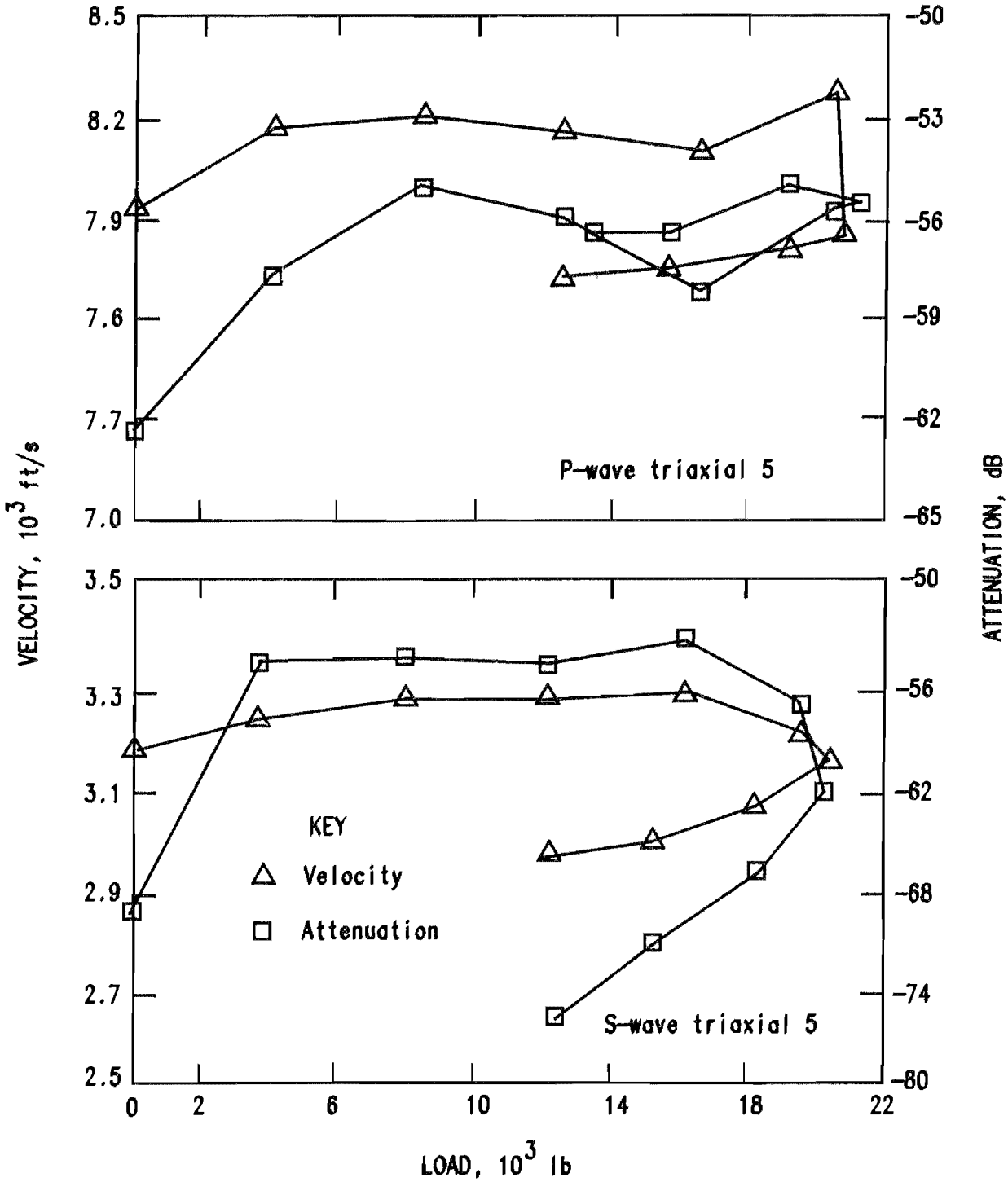

Figure A-7.—Velocity and attenuation of waves versus load for triaxial test 5, showing the three phases of behavior change as load increases and as failure occurs.

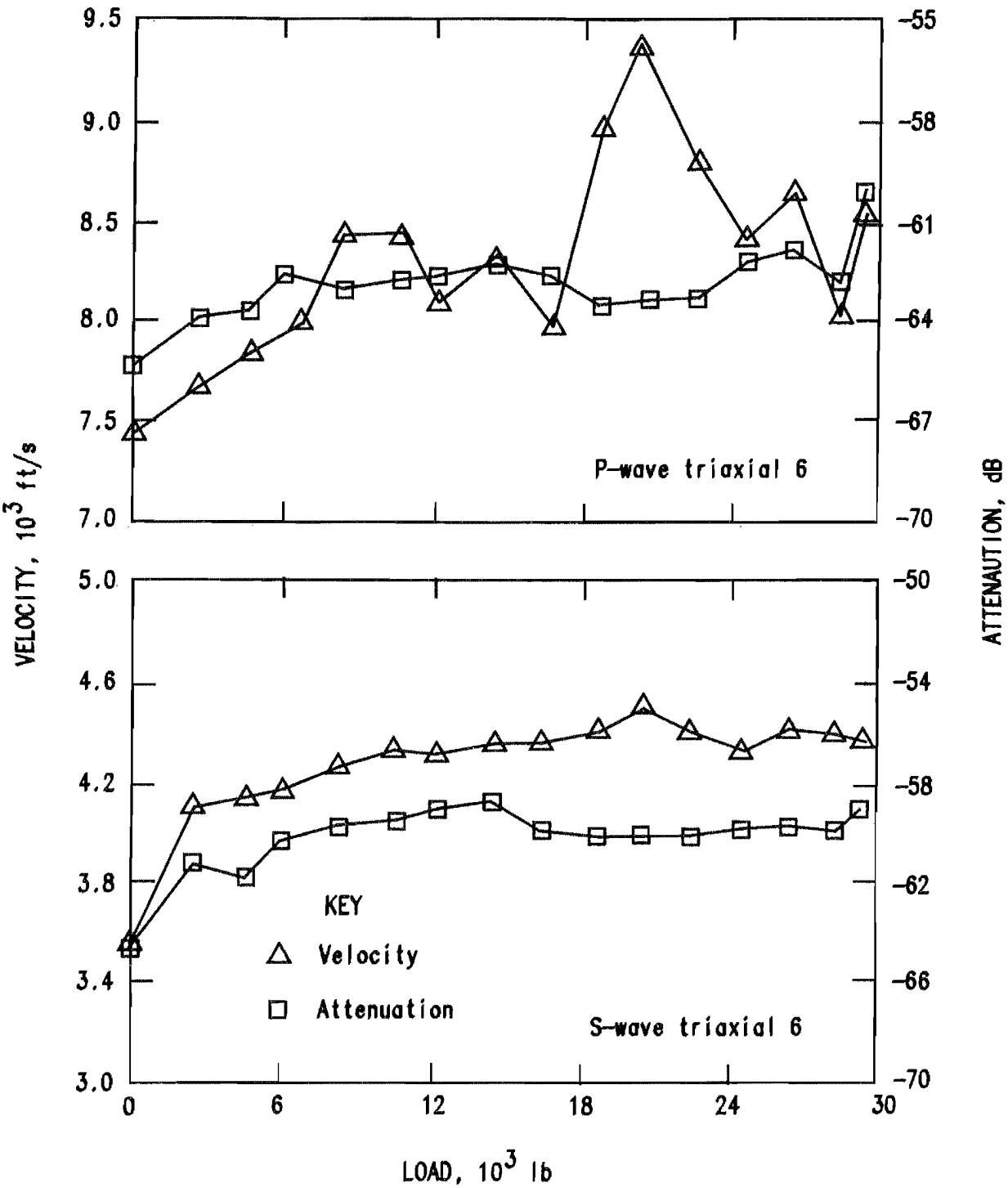

Figure A-8.—Velocity and attenuation of waves versus load for triaxial test 6, showing the three phases of behavior change as load increases and as failure occurs.

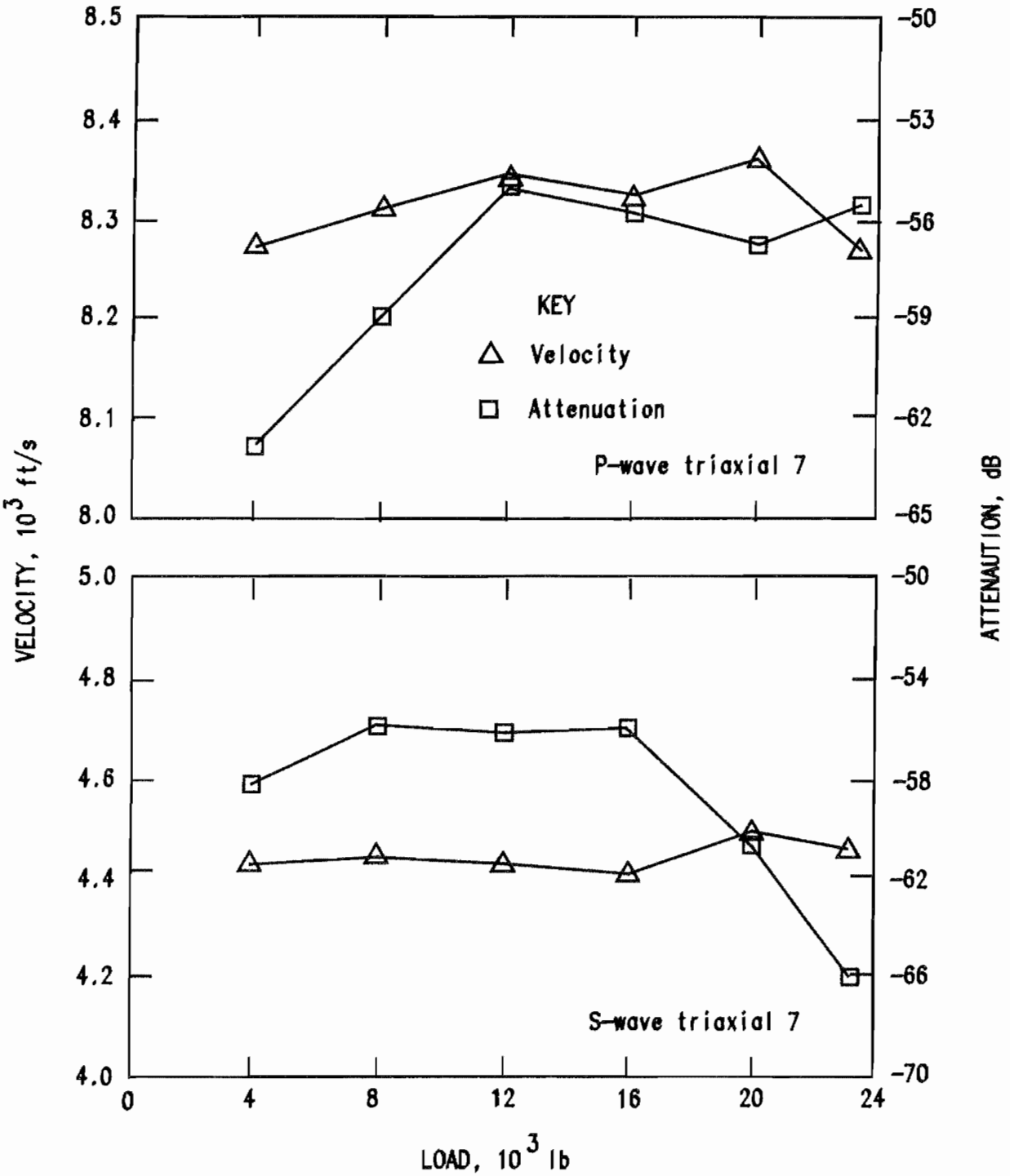

Figure A-9.—Velocity and attenuation of waves versus load for triaxial test 7, showing the three phases of behavior change as load increases and as failure occurs.

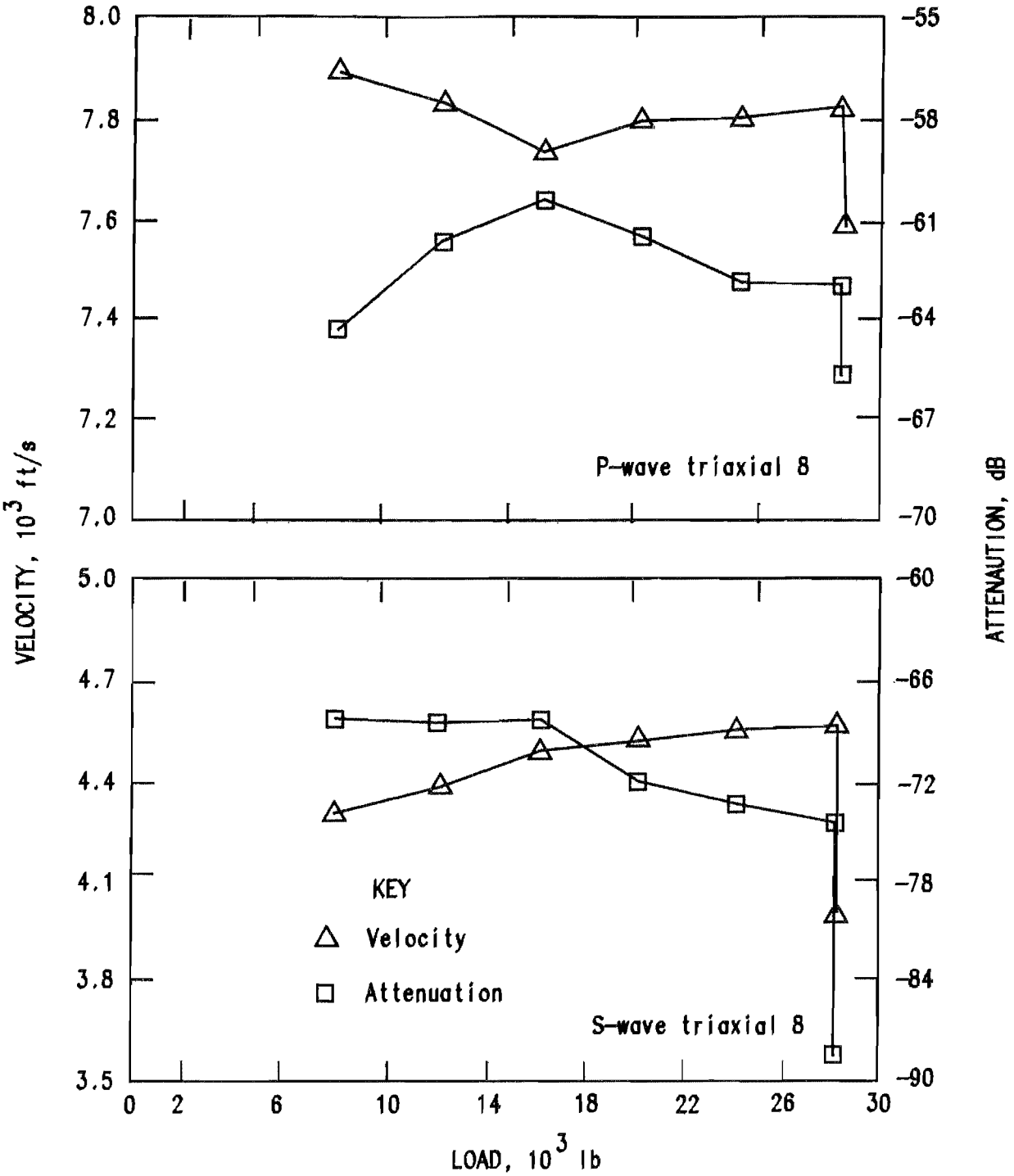

Figure A-10.—Velocity and attenuation of waves versus load for triaxial test 8, showing the three phases of behavior change as load increases and as failure occurs.

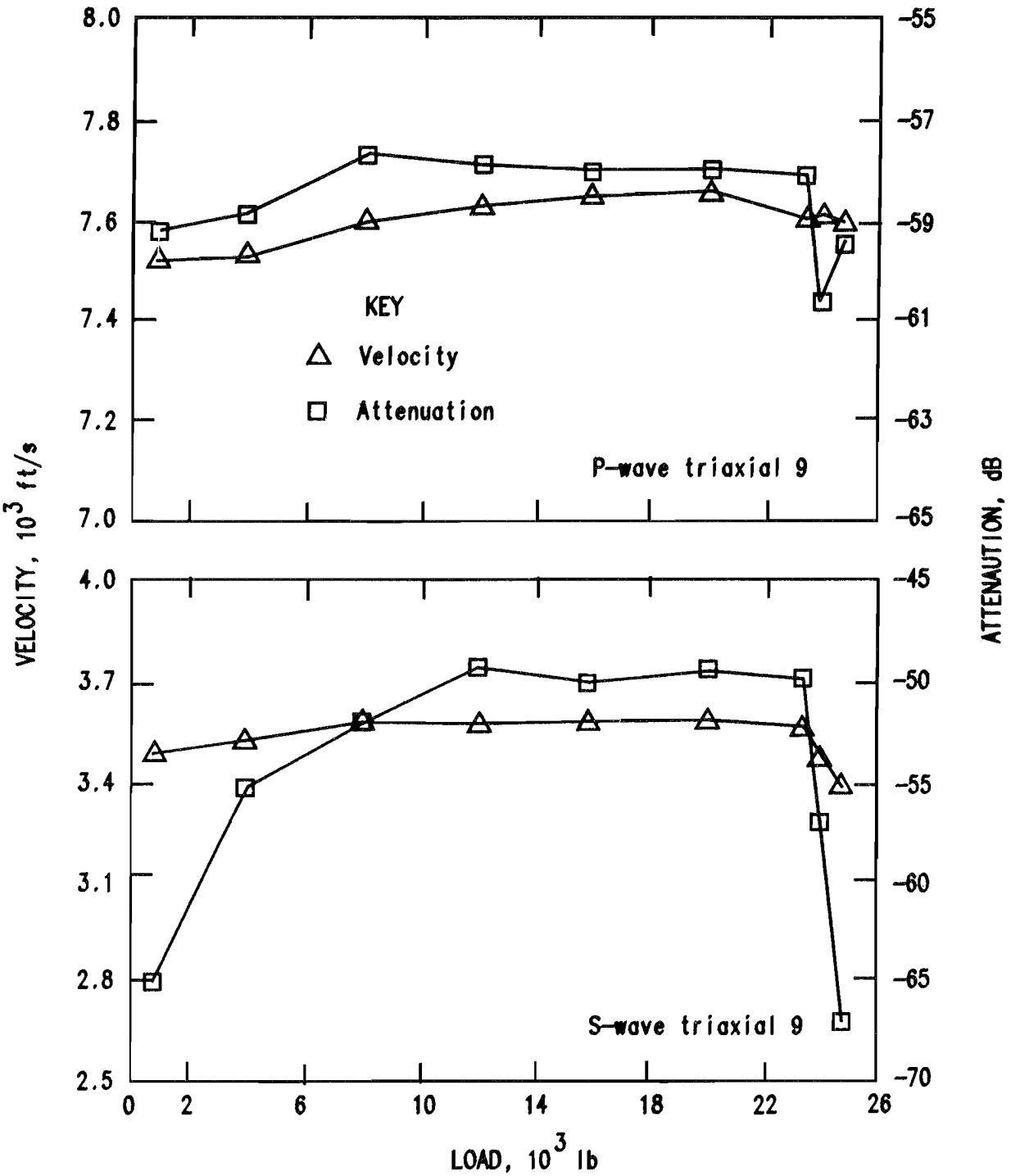

Figure A-11.—Velocity and attenuation of waves versus load for triaxial test 9, showing the three phases of behavior change as load increases and as failure occurs.

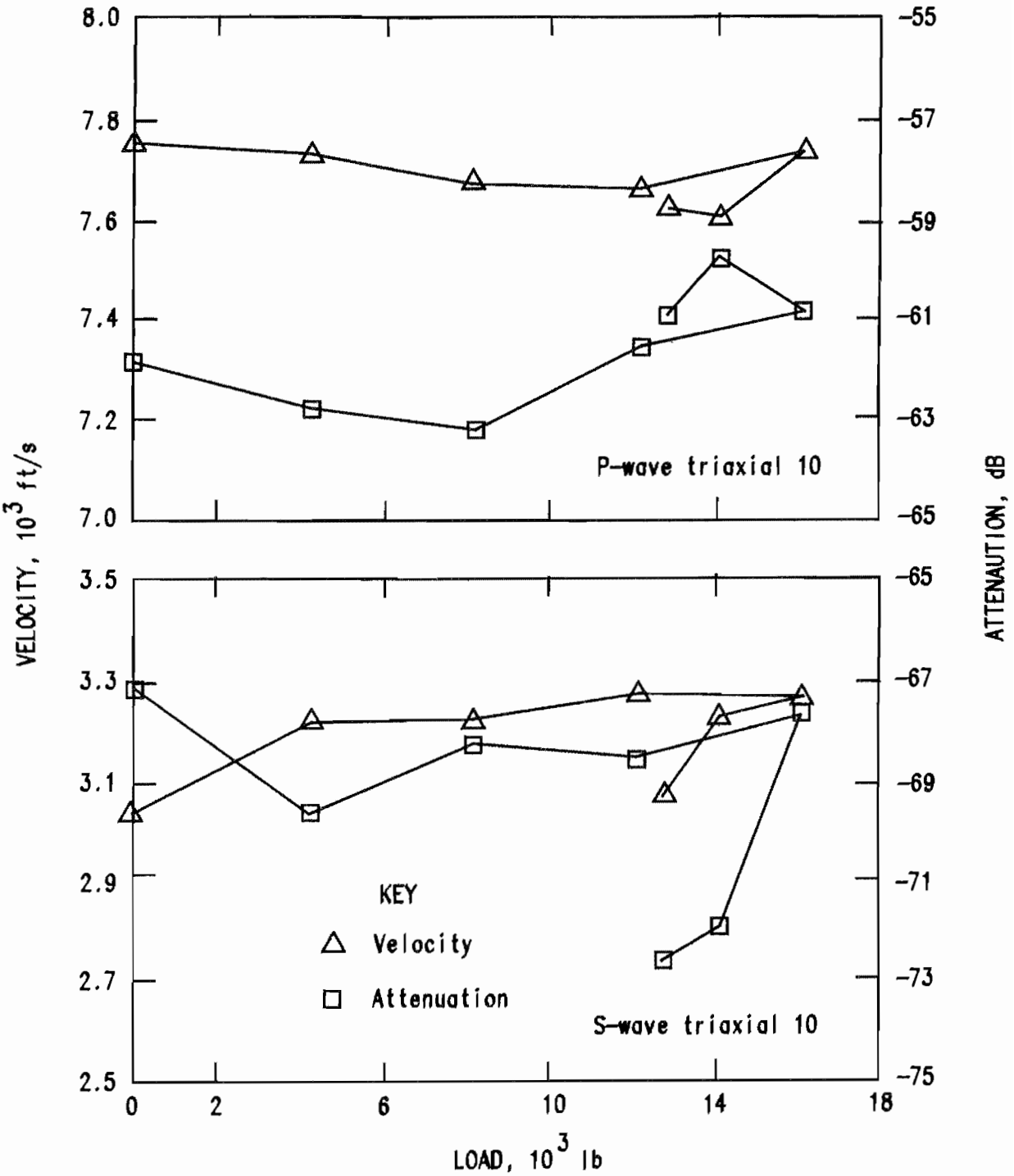

Figure A-12.—Velocity and attenuation of waves versus load for triaxial test 10, showing the three phases of behavior change as load increases and as failure occurs.

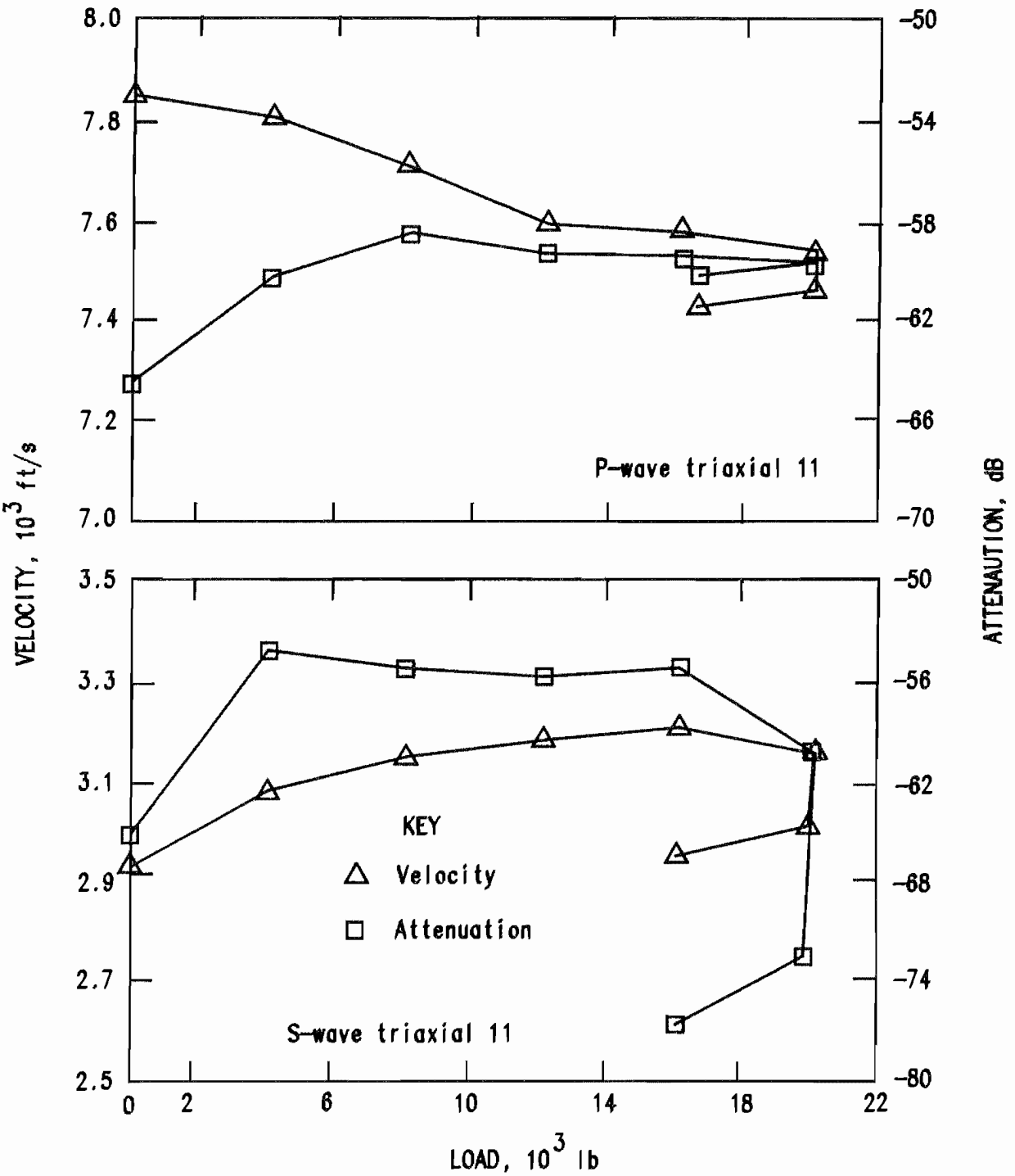

Figure A-13.—Velocity and attenuation of waves versus load for triaxial test 11, showing the three phases of behavior change as load increases and as failure occurs.

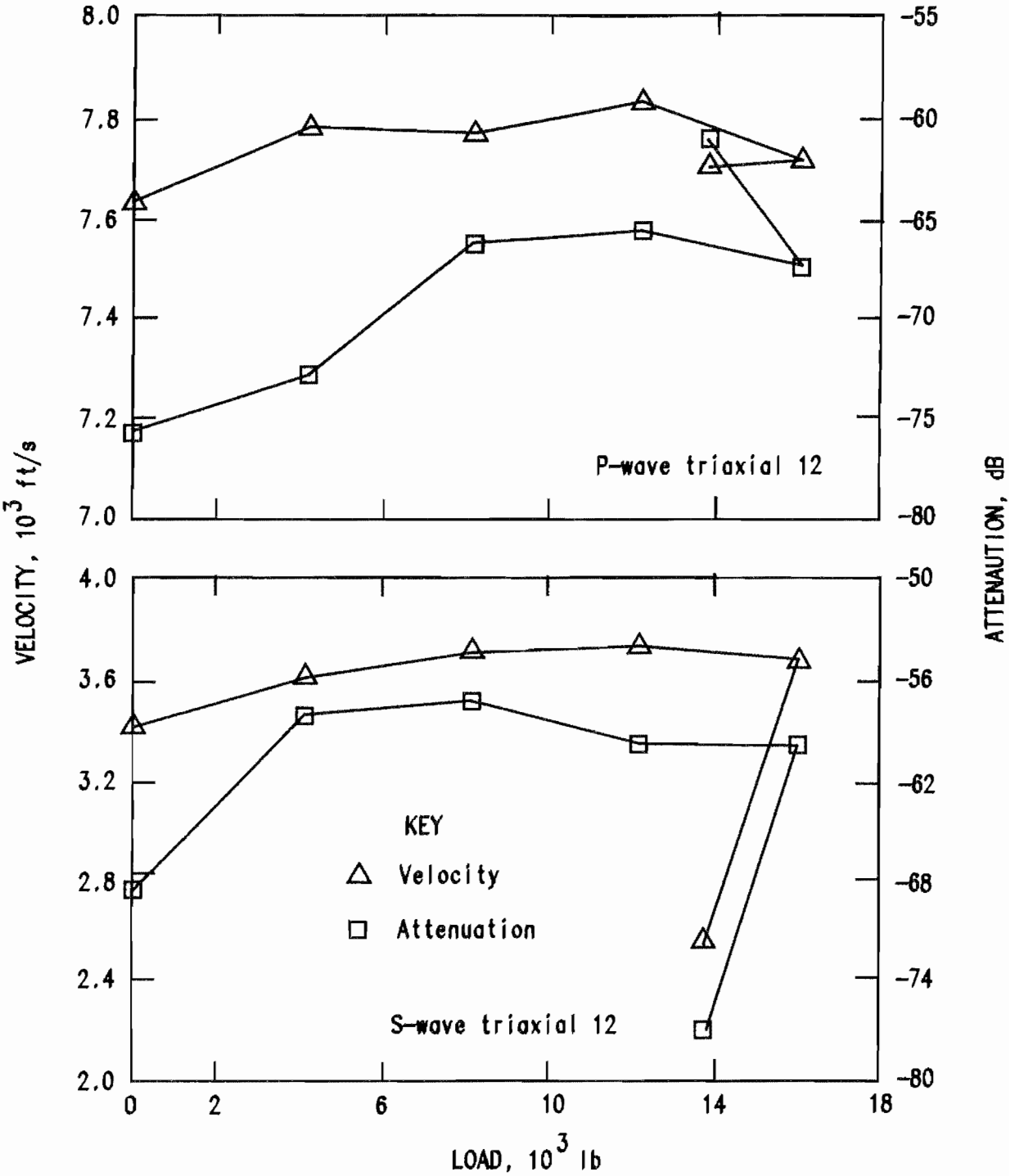

Figure A-14.—Velocity and attenuation of waves versus load for triaxial test 12, showing the three phases of behavior change as load increases and as failure occurs.

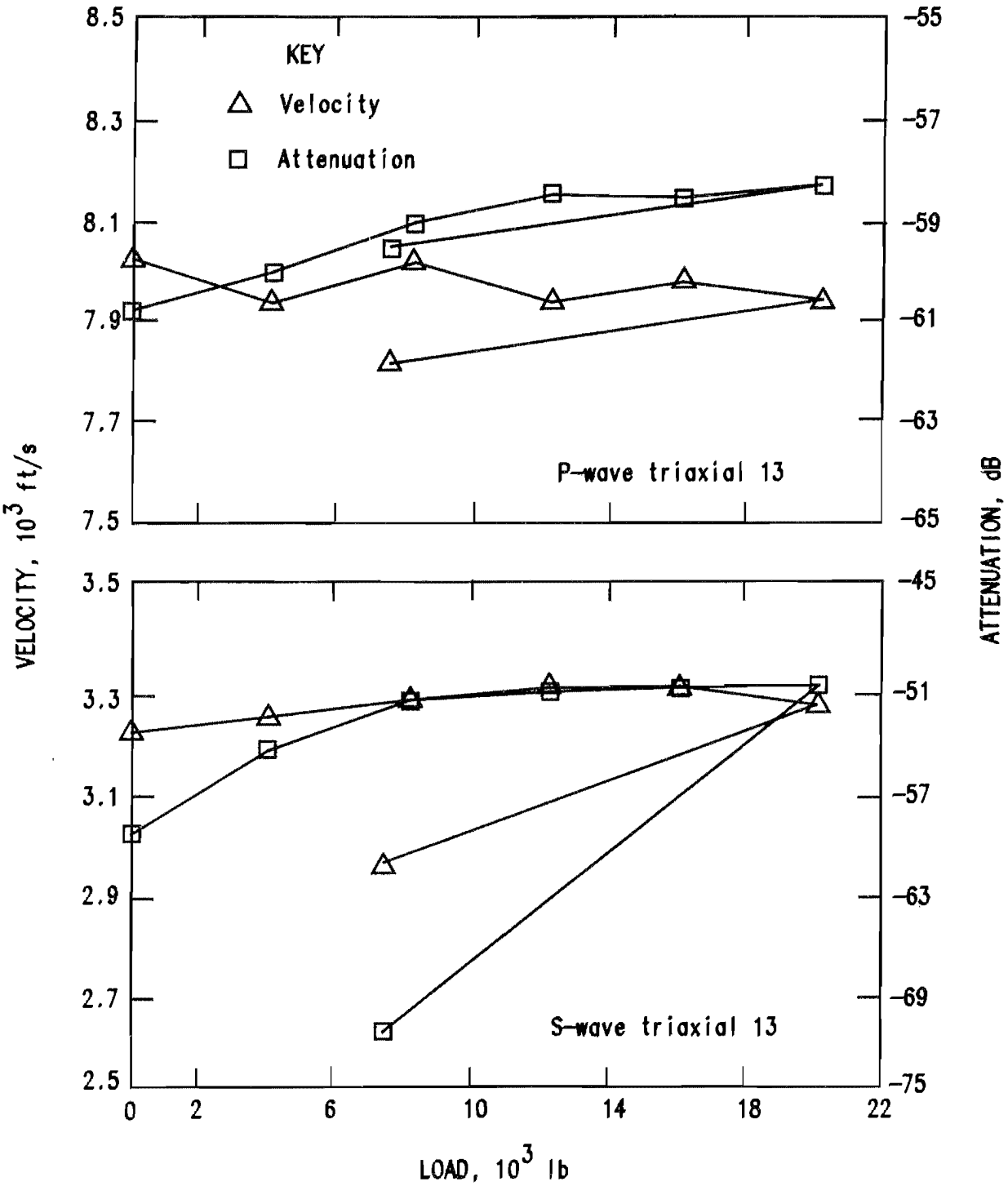

Figure A-15.—Velocity and attenuation of waves versus load for triaxial test 13, showing the three phases of behavior change as load increases and as failure occurs.

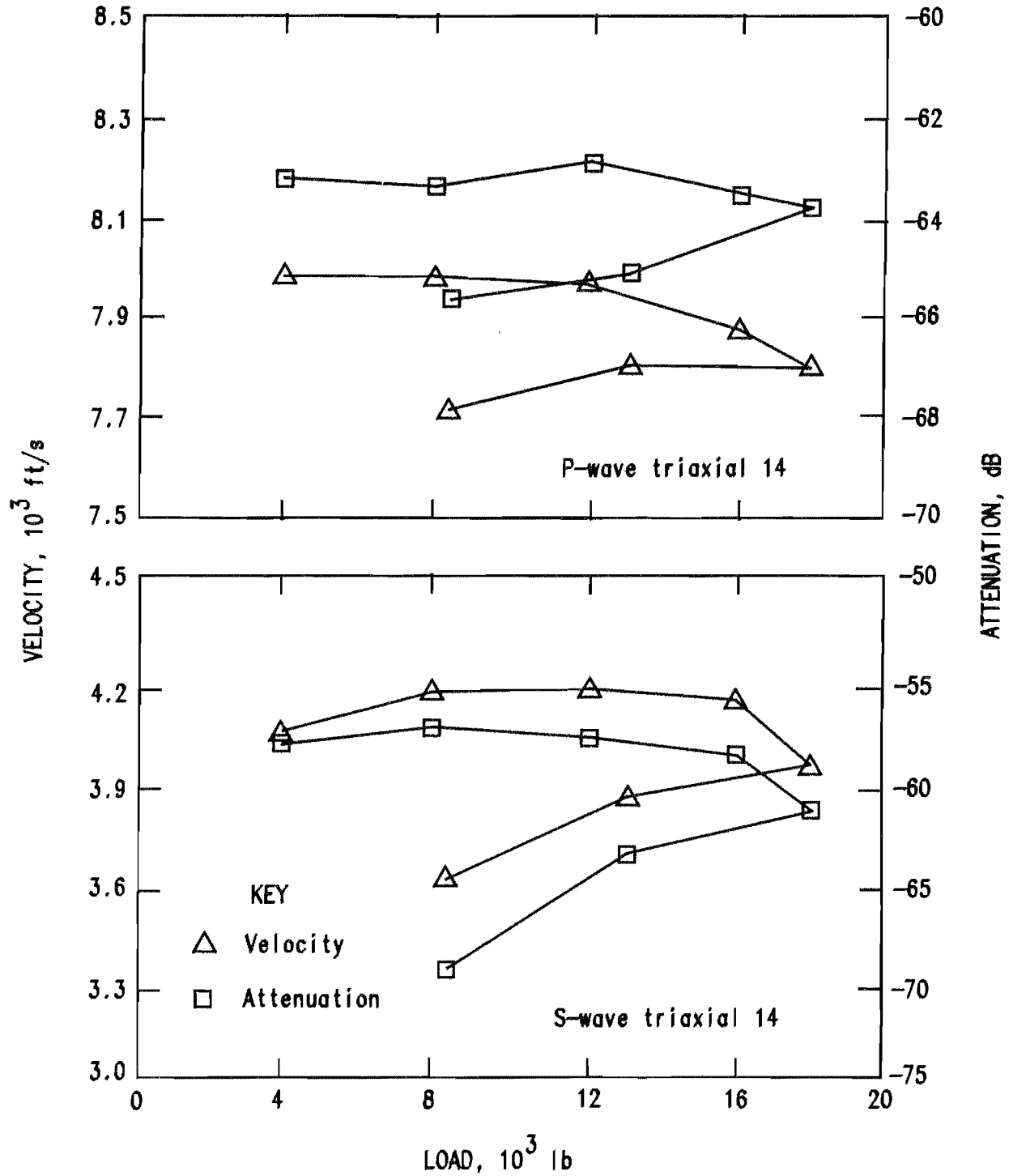

Figure A-16.—Velocity and attenuation of waves versus load for triaxial test 14, showing the three phases of behavior change as load increases and as failure occurs.

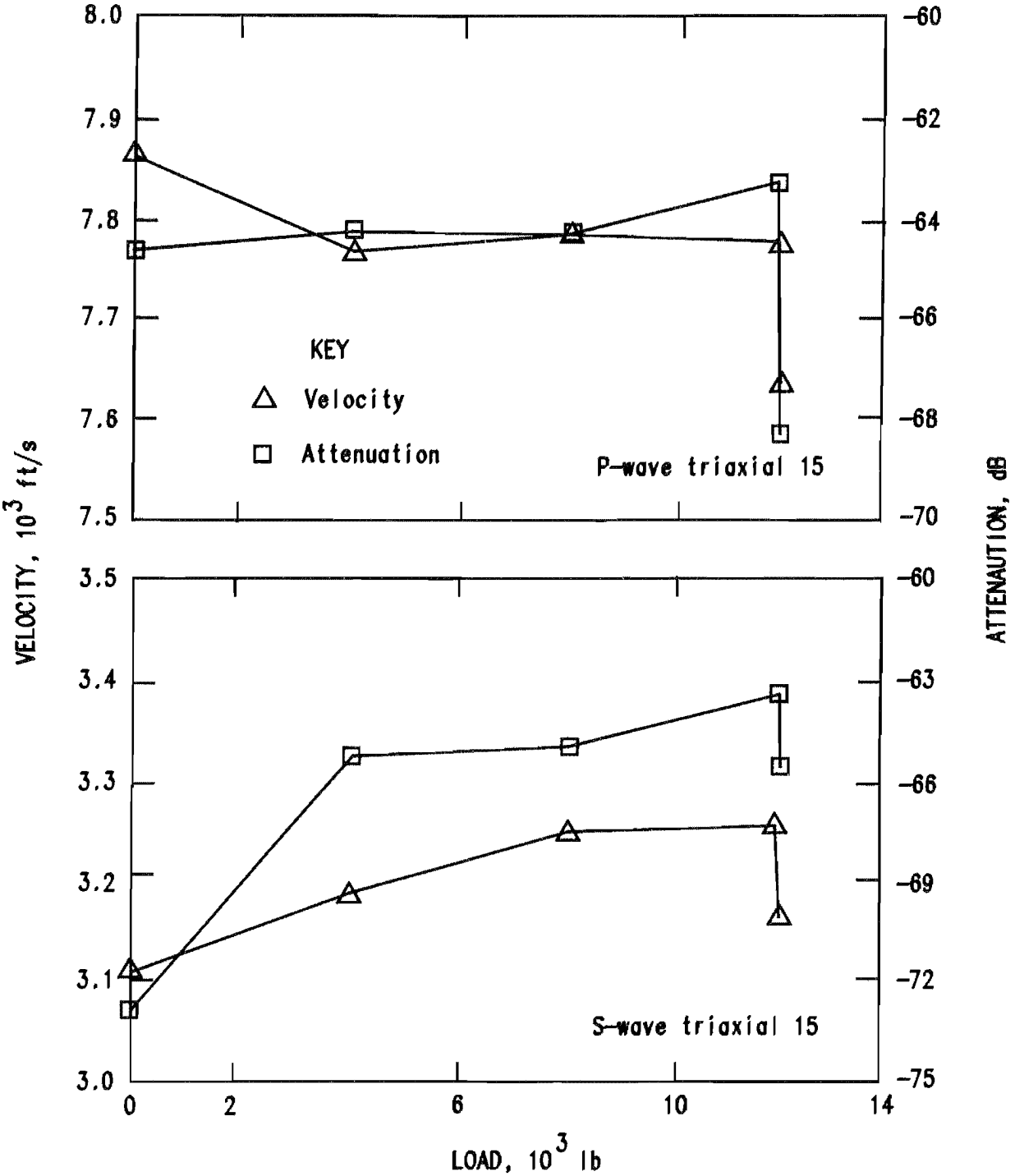

Figure A-17.—Velocity and attenuation of waves versus load for triaxial test 15, showing the three phases of behavior change as load increases and failure occurs.

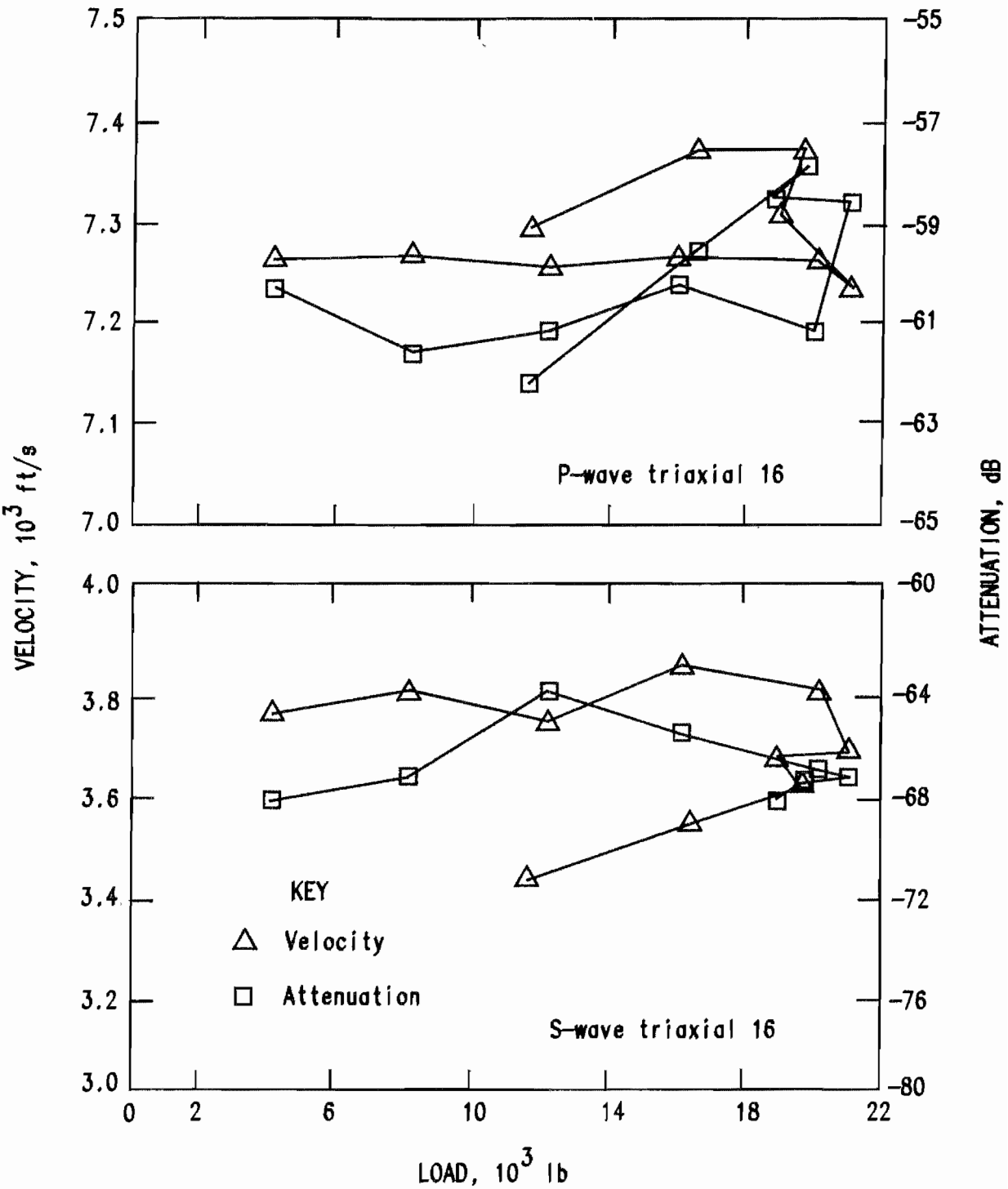

Figure A-18.—Velocity and attenuation of waves versus load for triaxial test 16, showing the three phases of behavior change as load increases and as failure occurs.

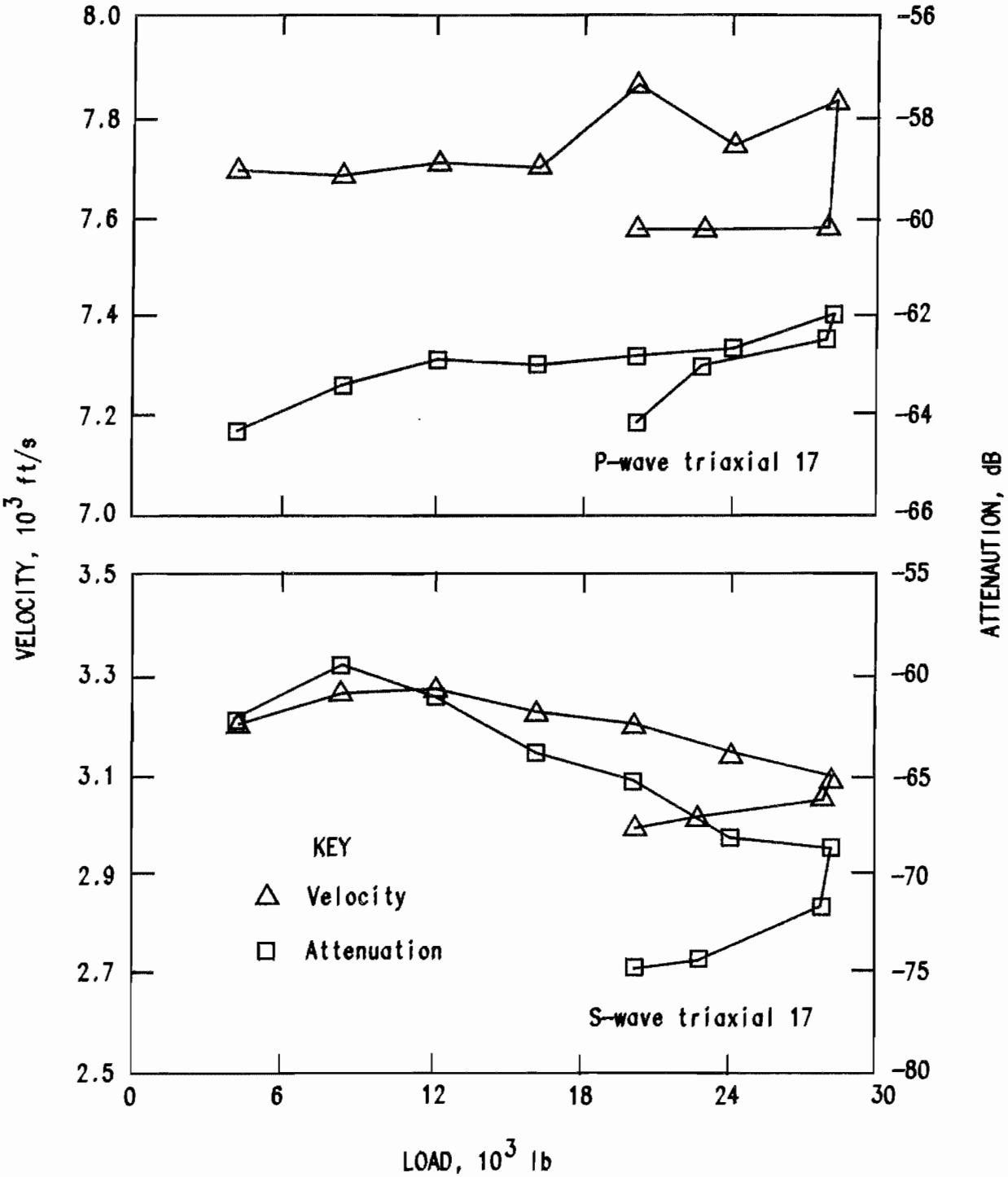

Figure A-19.—Velocity and attenuation of waves versus load for triaxial test 17, showing the three phases of behavior change as load increases and as failure occurs.

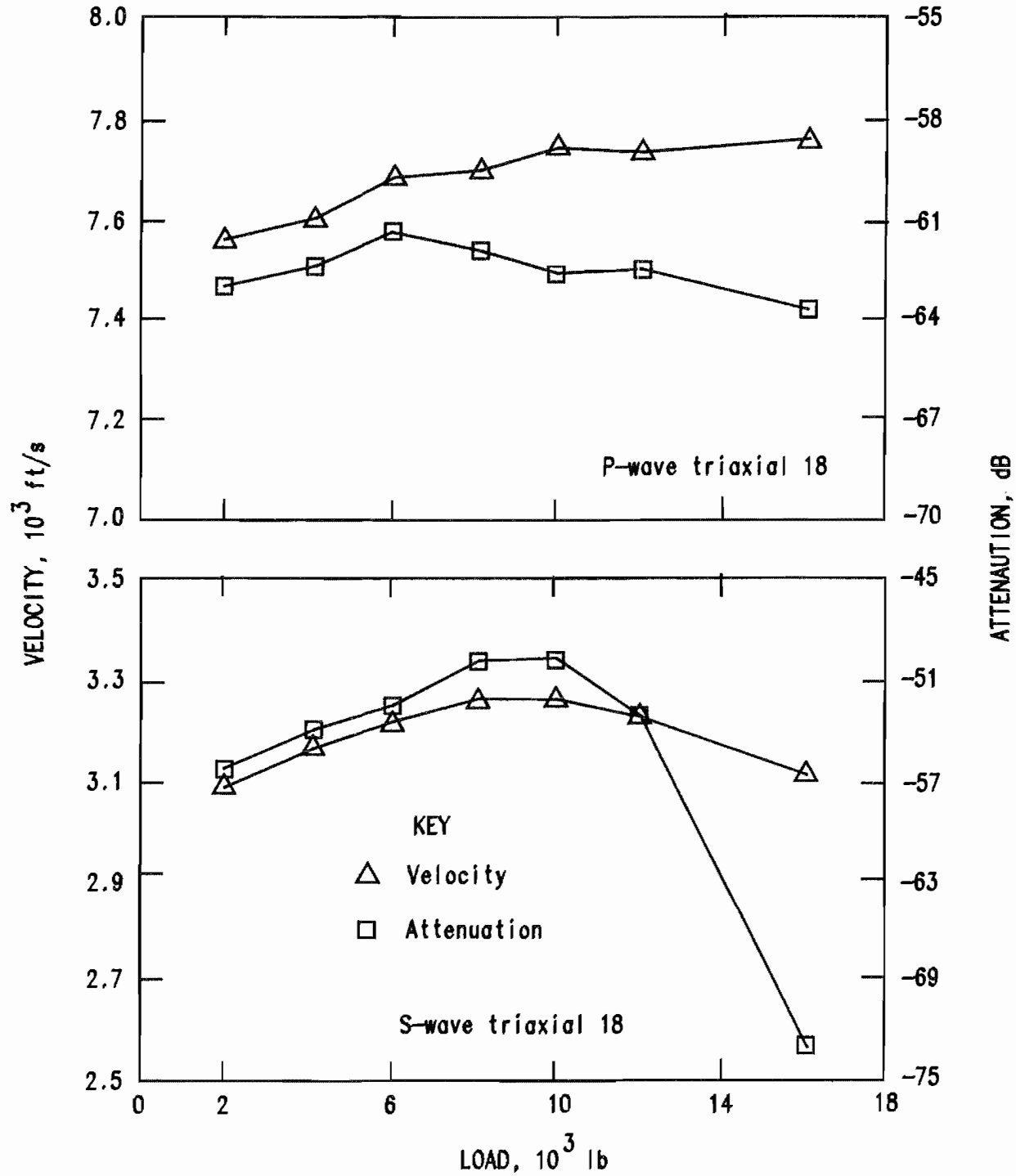

Figure A-20.—Velocity and attenuation of waves versus load for triaxial test 18, showing the three phases of behavior change as load increases and as failure occurs.

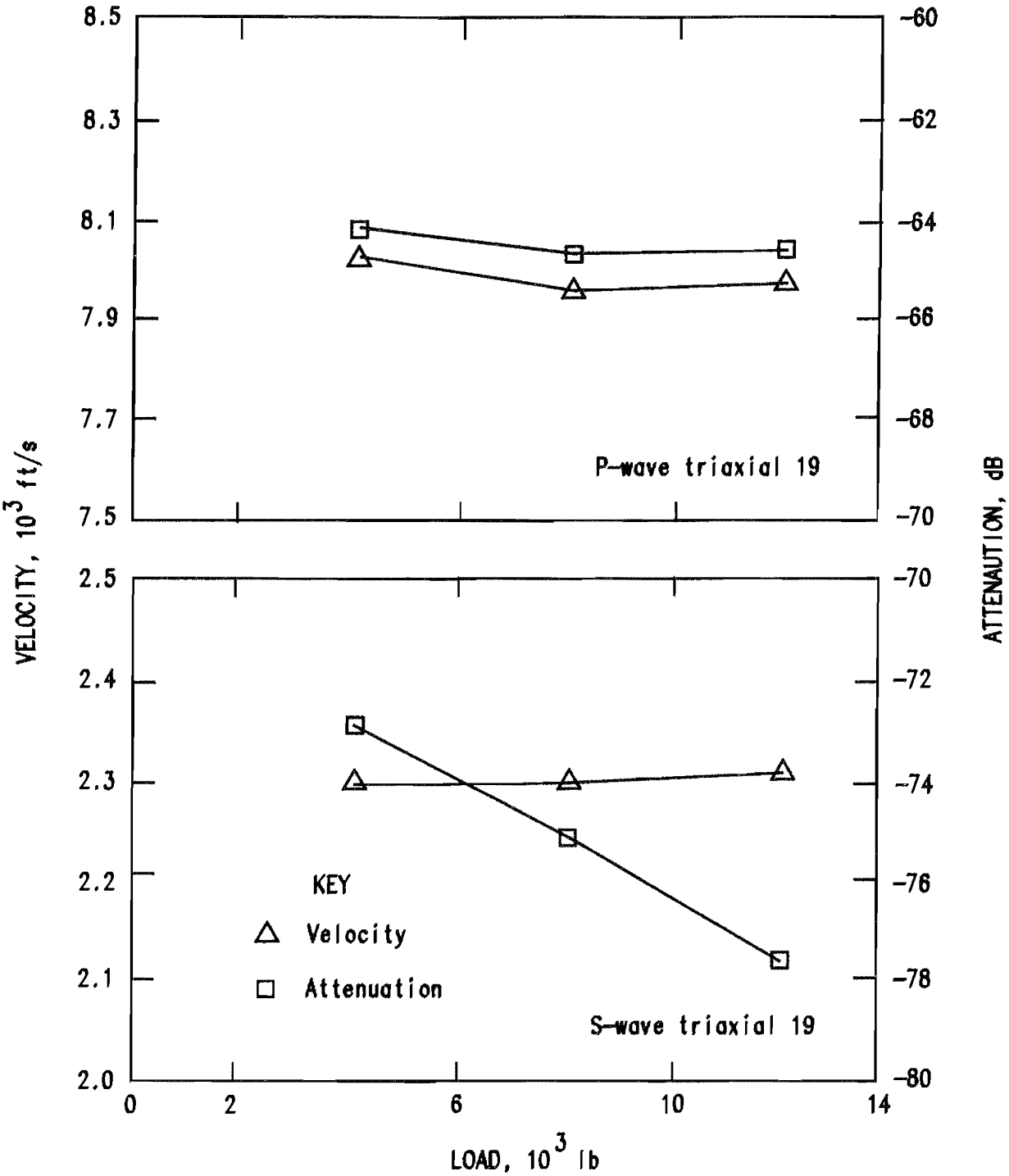

Figure A-21.—Velocity and attenuation of waves versus load for triaxial test 19, showing the three phases of behavior change as load increases and as failure occurs.

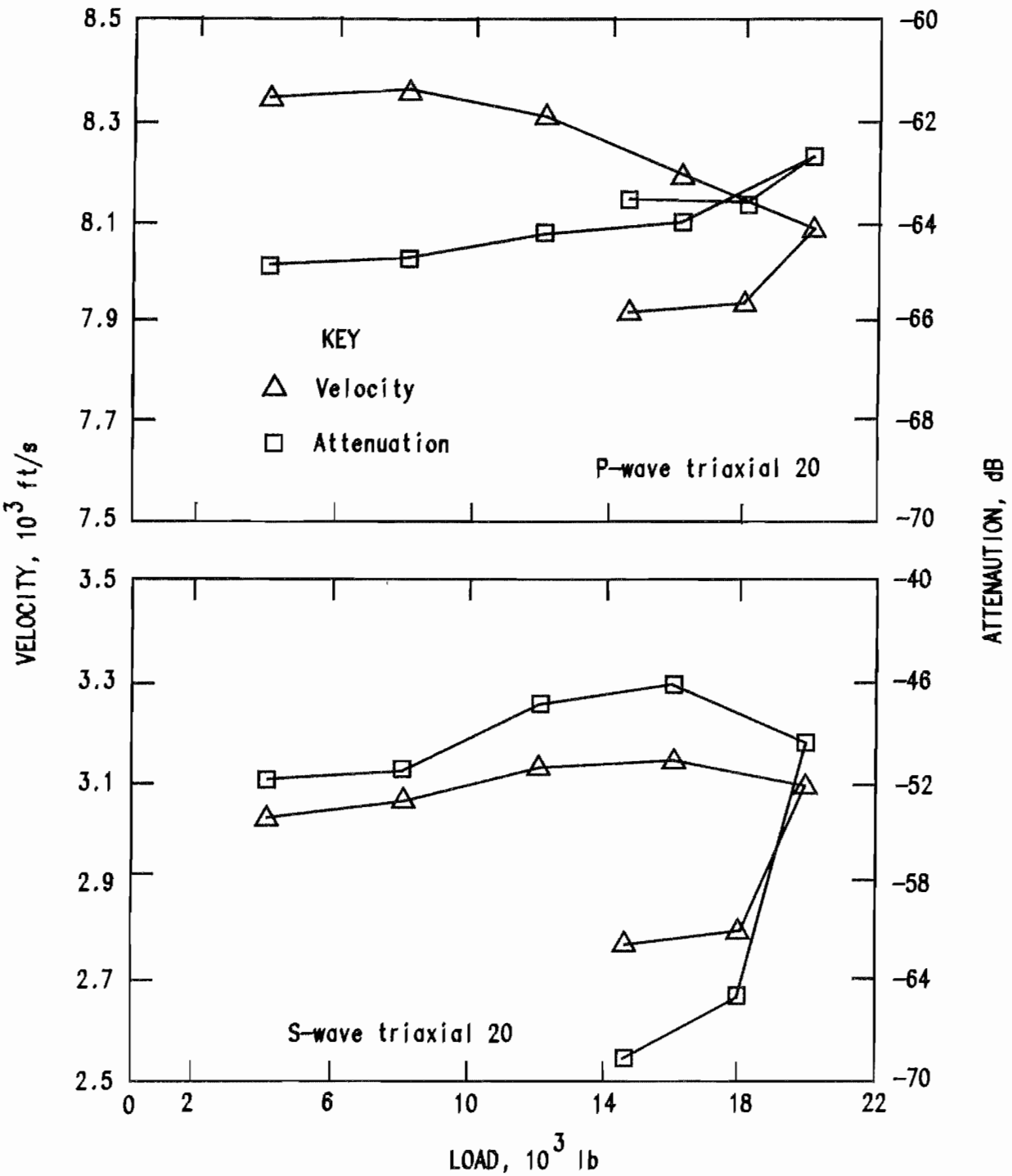

Figure A-22.—Velocity and attenuation of waves versus load for triaxial test 20, showing the three phases of behavior change as load increases and as failure occurs.

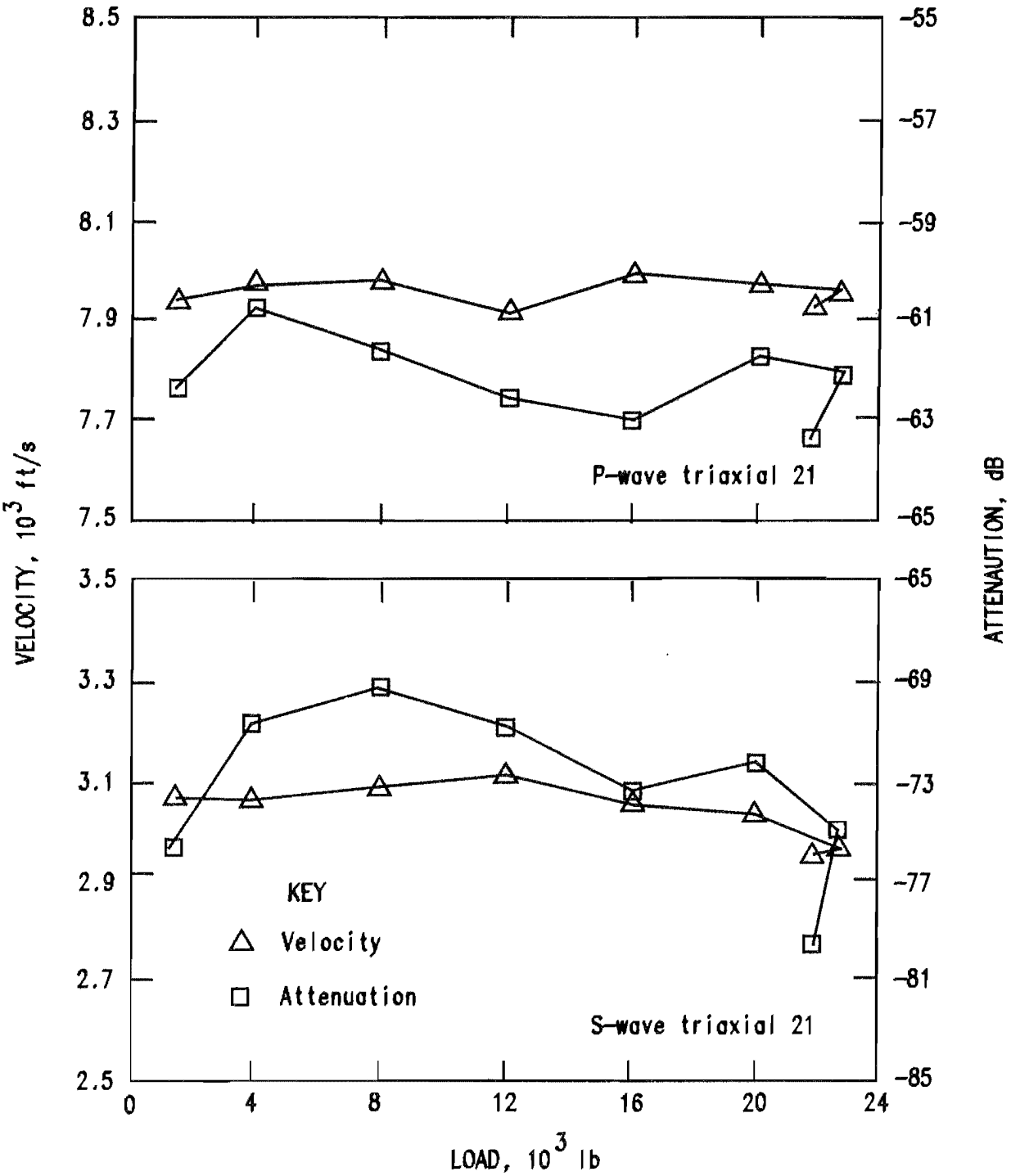

Figure A-23.—Velocity and attenuation of waves versus load for triaxial test 21, showing the three phases of behavior change as load increases and as failure occurs.

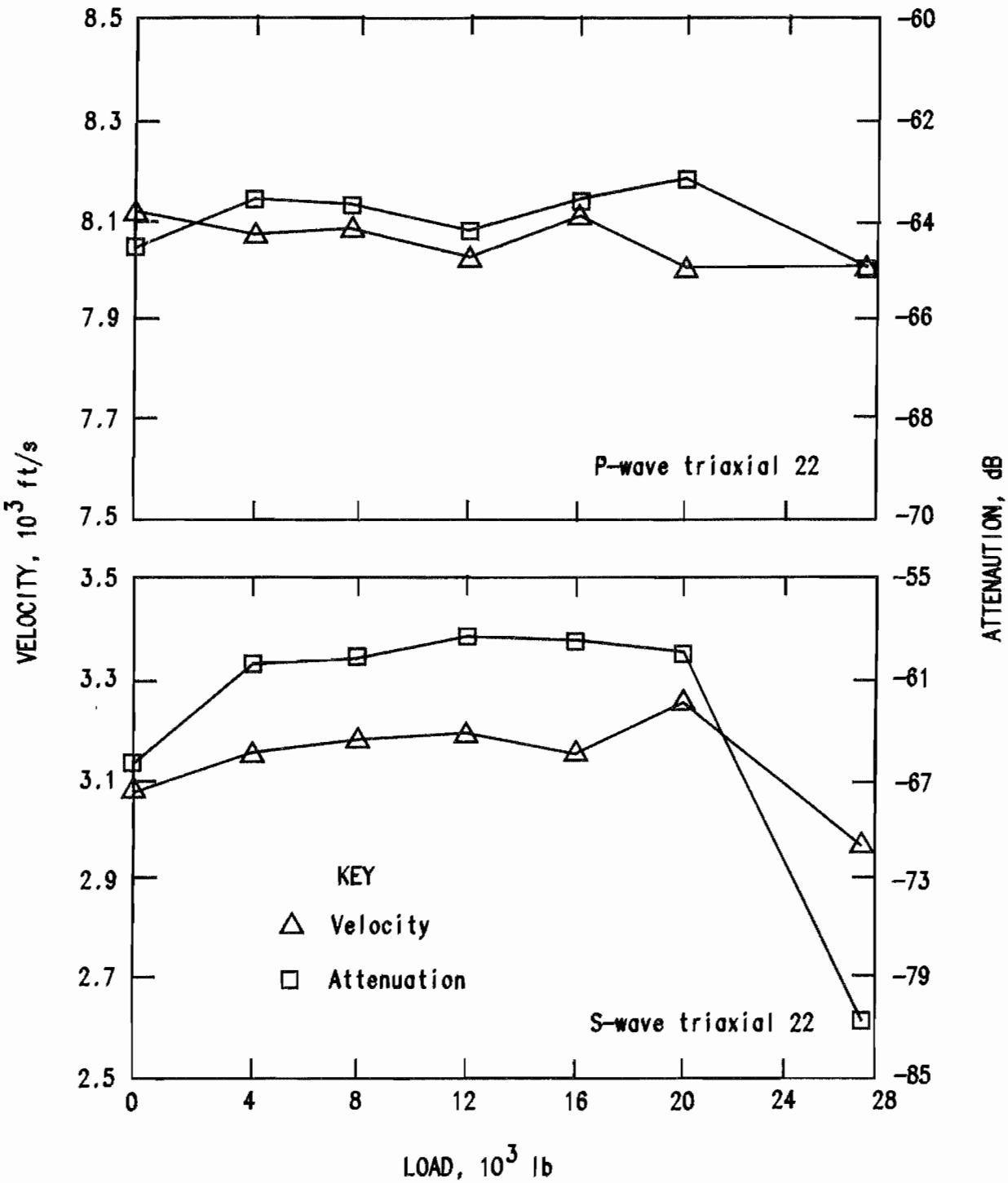

Figure A-24.—Velocity and attenuation of waves versus load for triaxial test 22, showing the three phases of behavior change as load increases and as failure occurs.

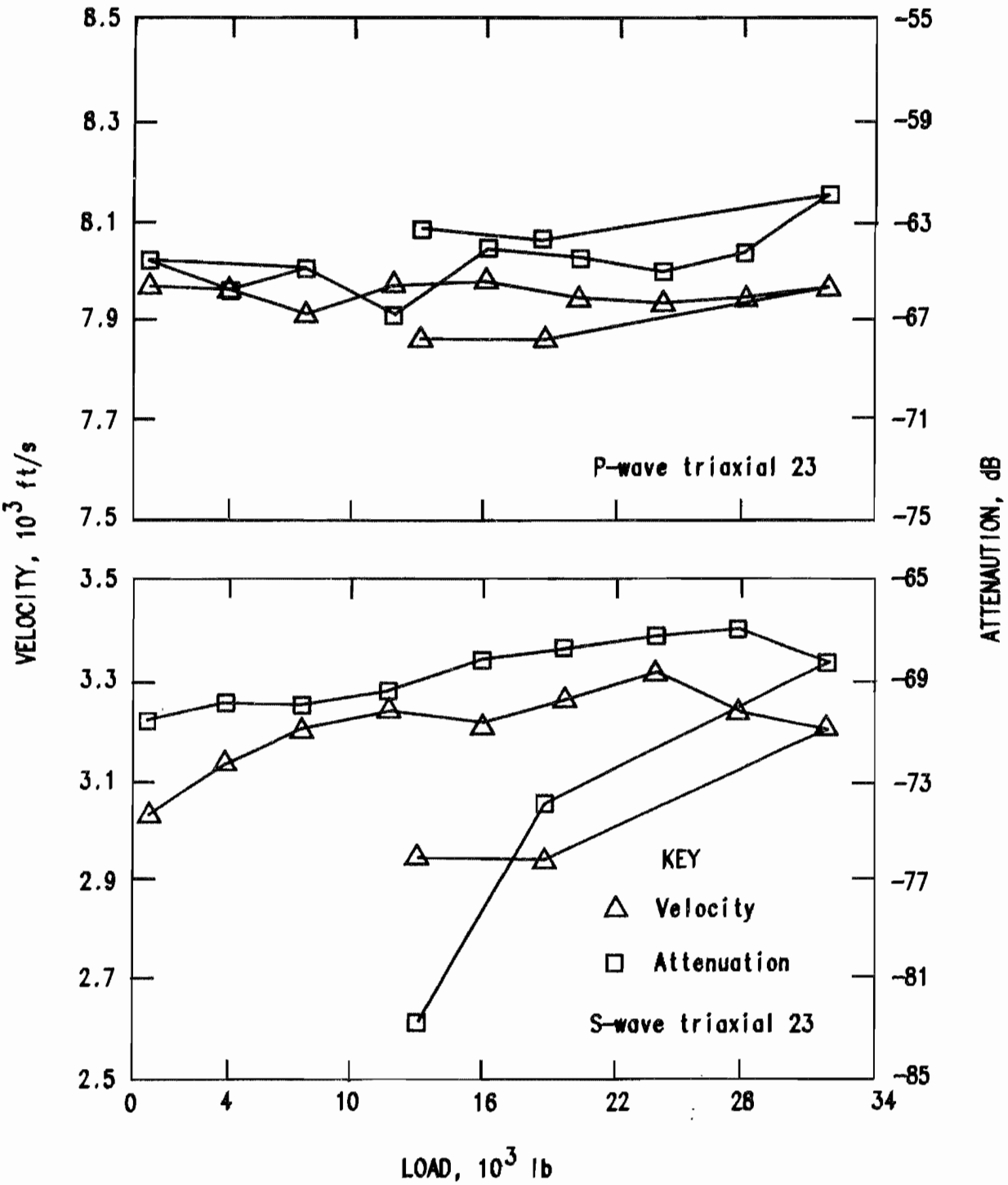

Figure A-25.—Velocity and attenuation of waves versus load for triaxial test 23, showing the three phases of behavior change as load increases and as failure occurs.

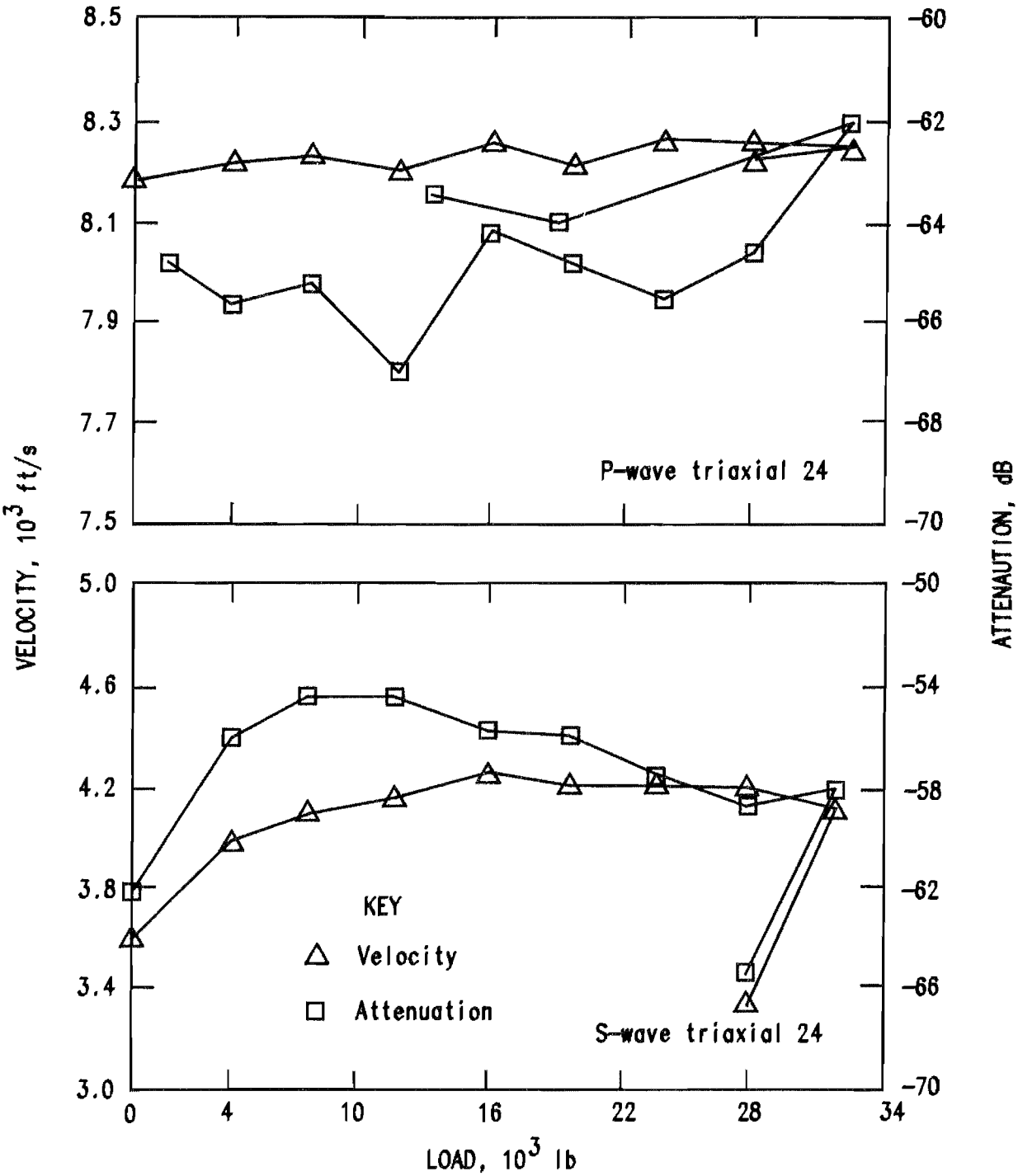

Figure A-26.—Velocity and attenuation of waves versus load for triaxial test 24, showing the three phases of behavior change as load increases and as failure occurs.

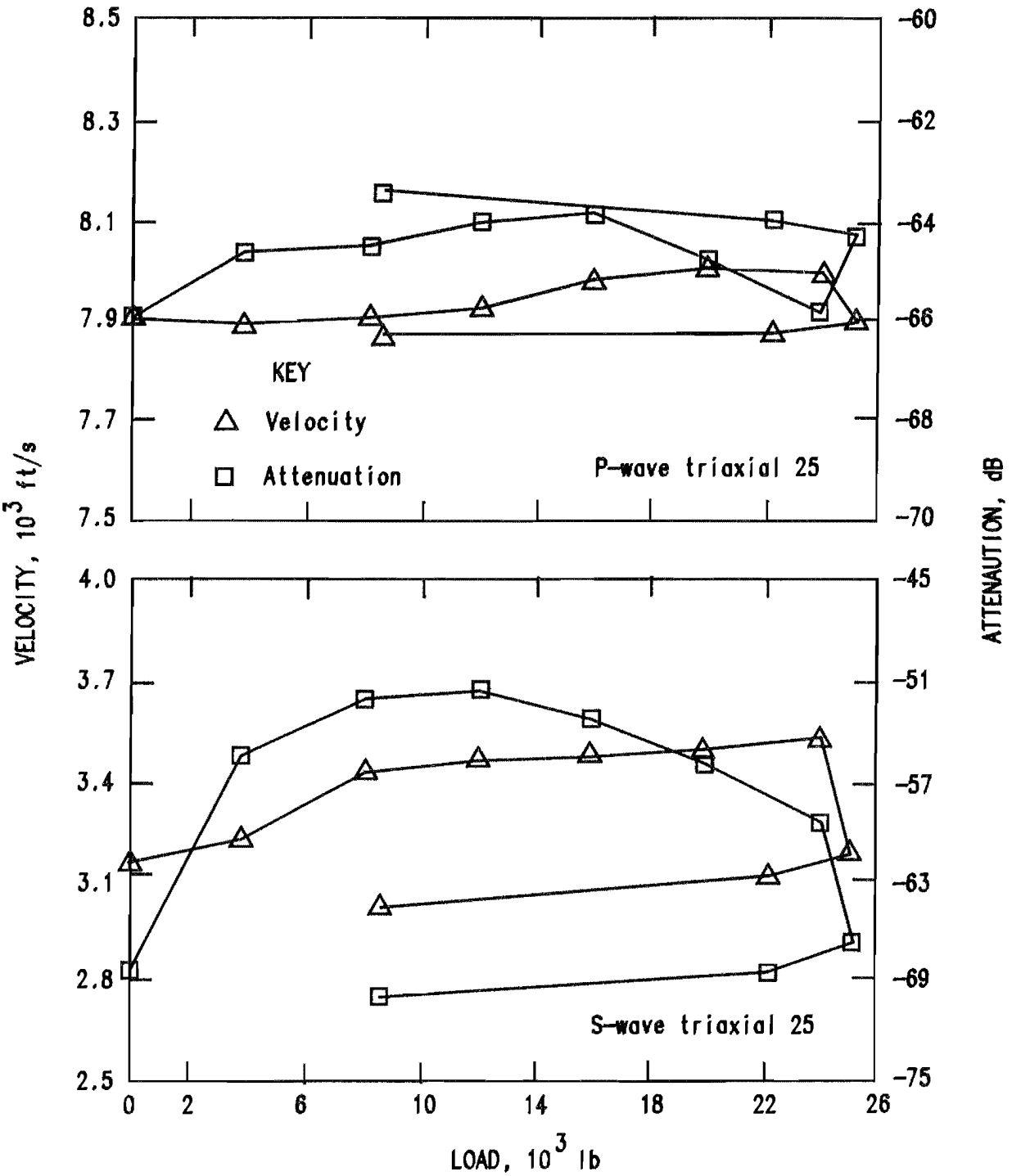

Figure A-27.—Velocity and attenuation of waves versus load for triaxial test 25, showing the three phases of behavior change as load increases and as failure occurs.